Available online at www.sciencedirect.com
ScienceDirect
Coordination Chemistry Reviews 251 (2007) 91–110
COORDINATION CHEMISTRY REVIEWS
www.elsevier.com/locate/ccr

Review

Recent advances in the coordination chemistry of diselenophosphates and allied ligands

Tarlok S. Lobana [a], Ju-Chun Wang [b], C.W. Liu [c,*]

[a] *Department of Chemistry, Guru Nanak Dev University, Amritsar 143005, India*
[b] *Department of Chemistry, Soochow University, Taipei 111, Taiwan*
[c] *Department of Chemistry, National Dong Hwa University, Hualien 974, Taiwan*

Received 13 January 2006; accepted 22 May 2006
Available online 2 June 2006

Contents

Abstract

This review describes the coordination chemistry of selenium containing ligands, namely, diselenophosphates [$(RO)_2PSe_2^-$, dsep], diselenophosphonates [$(R)(RO)PSe_2^-$, dsepo], diselenophosphinates [$R_2PSe_2^-$, dsepi], and triselenophosphonates [$RPSe_3^{2-}$, tsepo] with 'PSe_2' and 'PSe_3' functional groups. The coordination compounds of alkali metals, d-block elements, and p-block elements are discussed with respect to their formation and structural chemistry. These compounds are diverse ranging from mononuclear, dinuclear, and multinuclear complexes, to polymers. The important spectroscopic observations, bonding properties, substitution reactions, characteristics such as bond lability, the P–Se bond cleavage, co-crystallization, Se···Se interactions, oxophilicity, photophysical behavior, and metal selenide nanomaterial are also highlighted. The description of work is group by group and within a given metal, coordination compounds, if any, of all the ligands under purview are described. The literature survey is up to January 2006 and the review represents the first article in this area of research and should contribute considerable value for future research.

Keywords: Diselenophosphates; Diselenophosphinates; Diselenophosphonates; Triselenophosphonates; Metal complexes

1. Introduction

In this article, the coordination chemistry of phosphor-1,1-diselenoates, more commonly known as diselenophosphates [$(RO)_2PSe_2^-$, A], is reviewed. The coordination chemistry of diselenophosphates (abbreviated dsep) was initiated in 1968 by Zingaro et al. [1,2], but no significant work on metal complexes was reported until the late nineties [1–5]. In sharp contrast, many studies on the compositions and structures of phosphor-1,1-dithiolato metal complexes, clusters and polymers were reported [6–15]. In 1998 Liu et al. observed the cleavage of the P–Se bonds of dsep ligands for the first time during the reaction

* Corresponding author. Fax: +886 3 8633570.
E-mail address: chenwei@mail.ndhu.edu.tw (C.W. Liu).

0010-8545/$ – see front matter © 2006 Elsevier B.V. All rights reserved.
doi:10.1016/j.ccr.2006.05.010

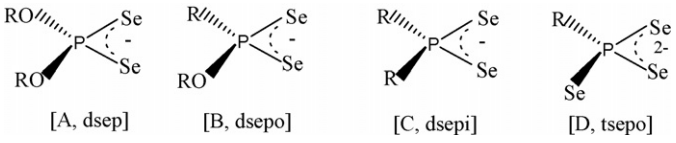

Chart 1.

with copper salts, leading to the formation of the selenium centered Cu_8 cubic clusters [16]. Since then a variety of complexes, clusters of other nuclearities, and polymers have been reported, making it imperative to review the work to provide impetus for future research.

Ligands similar to diselenophosphates, namely, diselenophosphonates [(R)(RO)PSe_2^-, B], diselenophosphinates [$R_2PSe_2^-$, C], and triselenophosphonates [$RPSe_3^{2-}$, D] are also included to provide a comparative analysis and comprehensive background for further investigation (Chart 1). Kuchen and Knop [17] were first to demonstrate the coordination chemistry of diselenophosphinates in 1965; and the first complex of a triselenophosphonate was reported in 1990 by Woollins and co-workers [18]. It was not until 2005 that the first reported synthesis of diselenophosphonates and their complexes was published by the Woollins's group [19].

One interesting property of dsep ligands is their ability to generate selenide-encapsulated clusters which may involve the rupture of P–Se bond. The interest in making clusters by a combination of transition metals and main group elements stems from several possibilities that such compounds could be precursors for the synthesis of new materials and provide a search for new coordination and geometries [20]. The synthesis of molecular cubic clusters having an interstitial main group atom is extremely rare [10,21–25] and is also interesting in view of their unusual bonding characteristics [26–32]. Furthermore copper clusters with chloride ion in the center have been used as the model to elucidate the possible role of D-penicillamine in chemotherapy for Wilson's disease [33,34]. The work reported is discussed groupwise for all four types of the ligands. Relatively more work has been reported with the dsep ligands than with allied ligands.

2. Ligands

Diselenophosphates (dsep, A) were isolated as alkali metal salts [1], or as their ammonium salts [16,35–38]. Diselenophosphonates (dsepo, B) were prepared from Woollins reagent $(PhPSe_2)_2$, by reacting with NaOR in ROH (R = Me, Et, ^{i}Pr) [19]. The reaction involved primarily the cleavage of the four-membered P_2Se_2 ring. Diselenophosphinates (dsepi, C) were obtained by the reaction of R_2PCl with Se powders, which initially forms $R_2P(Se)Cl$ then treatment with NaSeH yields $[R_2PSe_2]Na$ [17,39]. Triselenophosphonates (tsepo, D) were obtained as alkali metal salts, or produced in situ [18,40,41]. For example, reactions of $PhPCl_2$ with Na_2Se and Na_2Se_2 in a 1:1:1 molar ratio formed, $Na_2(PhPSe_3)$ [41], and dilithiation of a primary phosphine followed by reaction with three equiv of elemental selenium gave [$CyPSe_3Li_2{\cdot}2$ (tmeda)] (tmeda = $Me_2NCH_2CH_2NMe_2$) [40]. Chart 2 depicts various

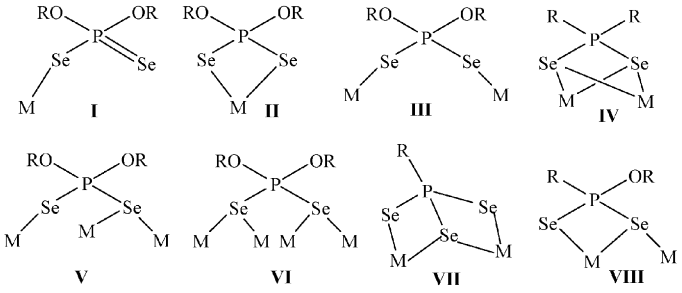

Chart 2.

coordination modes identified for diselenophosphates and allied ligands.

3. Survey of literature

The work is divided groupwise and all four types of the ligands are discussed together under a group where applicable. Coordination compounds of alkali metals, transition and main group elements are reported. Most of the investigations pertain to group 11 metals; metals of groups 10–12 are studied next in order and finally other metals including alkali metals are investigated to a small extent. Table 1 gives some important structural parameters for selected complexes.

3.1. Group 1 elements (Li, Na, K)

Only complexes of dsepi and tsepo ligands with lithium(I), sodium(I) and potassium(I), are reported [40,42,43]. The monomeric lithium complex [$Ph_2PSe_2Li{\cdot}$(thf)·(tmeda)], **1**, was obtained by two methods: (i) the first method involved treatment of *n*-BuLi with Ph_2PH, and tmeda ($Me_2NCH_2CH_2NMe_2$), followed by the addition of Se metal, and (ii) the second involved the reaction of Ph_2PH with *n*-BuLi in thf solvent in the presence of tmeda, followed by addition of one mole of Se metal, forming dimer $[Ph_2PSeLi{\cdot}(tmeda)]_2$, which was further treated with another mole of Se powder [40]. In compound **1**, the dsepi ligand is chelating, and the coordination number for Li is five with long and unequal Li–Se bonds, which may be due to both the higher coordination number of Li and weak bonding of the delocalized PSe_2^- moiety. ^{31}P NMR showed a single peak with a pair of satellites due to ^{31}P–^{77}Se coupling, which supports a single species in the solution state.

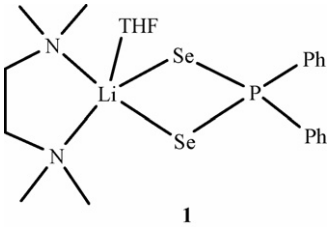

1

Another dsepi complex, $Na_2[Ph_2PSe_2]_2{\cdot}thf{\cdot}5H_2O$ **2**, obtained from Ph_2PCl and Na_xSe_y, is a polymeric structure consisting of a central core of fused and spiro Na_3O_3 rings [43]. One $Ph_2PSe_2^-$ acts as a unidentate ligand (η^1-Se, mode

Table 1
Structural parameters for selected complexes

Compound	M–X (range Å) (X = Se, Cl, Br, or O)	Bond Angles Se–M–Se (bite) (M–(μ_n-X)–M) X = Se, Cl, Br, O	Se···Se (average bite)	M···M	References
$[Ph_2PSe_2Li\cdot(thf)\cdot(tmeda)]$ **1**	2.848–2.940	77.38	–	–	[40]
$[K_2(Se_2PPh_2)_2(thf)_2]$ **3**	3.378–3.913	–	–	–	[42]
$[CyPSe_3Li_2(tmeda)_2]$ **4**	2.539–2.579	–	–	–	[40]
$Cp_2Ti(\eta^2\text{-}Se_2PPh_2)$ **5**	2.754–2.764	78.0	–	–	[44]
$[Mo_4(\mu_3\text{-}Se)_4\{Se_2P(O^iPr)_2\}_6]$ **6**	2.458–2.482 (μ_3-Se) 2.670–2.729	69.73–72.67 (μ_3-Se) 78.10–79.41	–	2.822–2.936	[49]
$[Mo_3(\mu_3\text{-}Se)(\mu\text{-}Se_2)_3\{Se_2P(O^iPr)_2\}_3]$ (Cl) **7**	2.491–2.496 (μ_3-Se) 2.642–2.692 2.603–2.625 (Se_{eq}) 2.518–2.541 (Se_{ax})	68.13–67.80 (μ_3-Se) 78.17–78.84		2.784–2.799	[49]
$[Mo_3(\mu_3\text{-}Se)(\mu\text{-}Se_2)_3\{Se_2P(OEt)_2\}_3]$ (Br) **8**	2.498–2.502 (μ_3-Se) 2.538–2.624 2.612–2.624 (Se_{eq}) 2.538–2.556 (Se_{ax})	78.60–79.00		2.783–2.790	[50]
$[Cp^*Ru(\eta^2\text{-}Se_2P^iPr_2)(\eta^2\text{-}SeP^iPr_2)]^+$ **9**	2.538–2.590	81.2	–	–	[52]
cis-$Pt\{Se_2(Se)PPh\}(dppe)$ **14**	2.465–2.471	85.3	3.34	–	[18]
$Pd[Se_2P(O^iPr)_2]_2$ **13**	2.440–2.456	86.23	3.545		[49]
$[Ni\{Se_2P(OMe)Ph\}_2]$ **12**	2.3547–2.355	89.87	–	–	[19]
$Cu_8(\mu_8\text{-}Se)[Se_2P(O^nPr)_2]_6\}$ **15b**	2.504–2.520 (μ_8-Se) 2.452–2.461	70.48–70.57 102.0–116.6	3.776	2.899–2.912	[59]
$\{Cu_8(\mu_8\text{-}Se)[Se_2P(O^iPr)_2]_6\}$ **15c**	2.506–2.577 (μ_8-Se) 2.447 (average μ_2-Se)	113.15–118.09	3.784	2.859–2.974	[16]
$[Cu_8(\mu_8\text{-}Cl)\{Se_2P(OEt)_2\}_6](PF_6)$ **16a**	2.649–2.775 (μ_8-Cl) 2.365–2.408	68.4–72.2 115.7–121.0	3.808	3.13 (average)	[63]
$[Cu_8(\mu_8\text{-}Cl)\{Se_2P(O^nPr)_2\}_6](PF_6)$ **16b**	2.674–2.878 (μ_8-Cl) 2.383–2.400	70.34–70.45 117.3–119.7	3.801	3.15 (average)	[63]
$[Cu_8(\mu_8\text{-}Cl)\{Se_2P(O^iPr)_2\}_6](PF_6)$ **16c**	2.691–2.743 (μ_8-Cl) 2.368–2.394	69.41–72.03 116.8–120.0	3.811	3.14 (average)	[63]
$\{Cu_8(\mu_8\text{-}Br)[Se_2P(OEt)_2]_6\}(PF_6)$ **17a**	2.695–2.797 (μ_8-Br) 2.360–2.404	68.28–72.06 116.2–121.3	3.807	3.192 (average)	[60]
$\{Cu_8(\mu_8\text{-}Br)[Se_2P(OPr^i)_2]_6\}(PF_6)$ **17c**	2.732–2.771 (μ_8-Br) 2.374–2.399	69.40–71.97 117.2–120.2	3.823	3.179 (average)	[36,60]
$Cu_{11}(\mu_9\text{-}Se)(\mu_3\text{-}Br)_3[Se_2P(O^iPr)_2]_6$ **18c**	2.519–2.748 (μ_9-Se) 2.350–2.502 2.541 (average μ_3-Br)	65.12–144.15 69.18–73.96 (Cu–Br–Cu)	3.731	2.787–2.970	[36,60]
$Cu_{11}(\mu_9\text{-}Se)(\mu_3\text{-}I)_3[Se_2P(O^iPr)_2]_6$ **19c**	2.500–2.766 (μ_9-Se) 2.358–2.504 2.692 (average μ_3-I)	62.57–144.03 62.51–71.59 (Cu–I–Cu)	3.727	2.805–3.154	[59]
$[Cu_{12}(P_2Se_6)[Se_2P(OEt)_2]_8]$ **20**	2.352–2.556 2.338–2.657 (P_2Se_6-Cu)	99.89–122.86 90.67–124.98	–	2.610–2.917	[37]
$Cu_8(\mu_8\text{-}Se)[S_2P(OEt)_2]_6$ **21**	2.539–2.624 (μ_8-Se) 2.275–2.342 (μ_2-S)	69.68–71.39 116.70–122.47	3.478 (S···S)	2.950, 3.062	[66]
$Cu_4[Se_2P(O^iPr)_2]_4$ **23**	2.354–2.408	102.0–129.1	3.719	2.711–2.899	[58]
$\{Ag_8(\mu_8\text{-}Se)[Se_2P(O^iPr)_2]_6\}$ **24**	2.714–2.868 (μ_8-Se) 2.535–2.633	69.40 115.80–122.62	3.771	3.180–3.358	[35]
$[Ag_8(\mu_8\text{-}Cl)\{Se_2P(OEt)_2\}_6](PF_6)$ **26a**	2.809–2.978 (μ_8-Cl) 2.588–2.635	67.6–72.6 115.44–120.81	3.805	3.351 (average)	[68]
$[Ag_8(\mu_8\text{-}Cl)\{Se_2P(O^nPr)_2\}_6](PF_6)$ **26b**	2.853–3.020 (μ_8-Cl) 2.600–2.611	70.55 (average) 117.2–119.6	3.809	3.344	[68]
$[Ag_8(\mu_8\text{-}Br)\{Se_2P(OEt)_2\}_6](PF_6)$ **27a**	2.865–3.012 (μ_8-Br) 2.595–2.639	67.53–72.89 116.19–123.26	3.814	3.269–3.549	[68]
$[Ag_8(\mu_8\text{-}Br)\{Se_2P(O^nPr)_2\}_6](PF_6)$ **27b**	2.911–3.072 (μ_8-Br)	70.53 (average)	3.818	3.409 (average)	[68]

Table 1 (*Continued*)

Compound	M–X (range Å) (X = Se, Cl, Br, or O)	Bond Angles Se–M–Se (bite) (M–(μ_n-X)–M) X = Se, Cl, Br, O	Se···Se (average bite)	M···M	References
	2.608–2.617	117.53–119.79			
$[Ag_{10}(\mu_{10}\text{-Se})\{Se_2P(OEt)_2\}_8]$ **28a**	2.631–3.187 (μ_{10}-Se) 2.557–2.801	61.30–170.47	3.712	2.977–3.378	[38]
$[Ag\{Se_2P(O^iPr)_2\}]_6$ **29c**	2.594–2.678	93.91–132.94	–	3.047–3.152	[38]
$[Ag_{11}(\mu_9\text{-Se})(\mu_3\text{-I})_3\{Se_2P(O^iPr)_2\}_6]$ **30c**	2.696–3.157 (μ_9-Se) 2.548–2.709 2.880 (average μ_3-I)	61.86–144.08 94.75–119.69 63.95–68.32 (Ag–I-Ag)	3.757	3.023–3.367	[69]
$[Zn_4(\mu_4\text{-Se})\{Se_2P(O^nPr)_2\}_6]$ **31b**	2.345–2.495 (μ_4-Se) 2.460–2.640	106.9–112.0 102.9–115.5	3.694		[71]
$[Zn_4(\mu_4\text{-O})\{Se_2P(OEt)_2\}_6]$ **32a**	1.971–2.009 (μ_4-O) 2.437–2.508	108.7–110.3 105.7–107.5	3.647		[72]
$[Zn_4(\mu_4\text{-O})\{Se_2P(O^nPr)_2\}_6]$ **32b**	1.978–2.018 (μ_4-O) 2.466–2.501	108.9–110.1 102.9–107.3	3.630		[72]
$[Zn_4(\mu_4\text{-O})\{Se_2P(O^iPr)_2\}_6]$ **32c**	1.971–2.009 (μ_4-O) 2.403–2.525	107.7–111.1 102.5–109.8	3.634		[72]
$[Zn_2\{Se_2P(O^iPr)_2\}_4]$ **33c**	2.422–2.524	88.85–122.78	3.570		[70]
$[Zn\{Se_2P(OEt)_2\}_2]_n$ **33a**	2.456–2.514	89.15–97.70	3.494		[70]
$[Cd\{Se_2P(OEt)_2\}_2]_n$ **34a**	2.680	103.29–122.69	3.804		[72]
$[Cd_2\{Se_2P(O^iPr)_2\}_4]$ **34c**	2.598–2.712	82.58–123.31	3.576		[72]
$[Hg\{Se_2P(O^iPr)_2\}_2]_n$ **35c**	2.544–2.869	81.55–127.48	3.578		[72]
$[Cd_2\{Se_2P(OMe)Ph\}_4]$ **36a**	2.634–2.731	82.9	–	–	[19]
$In[Se_2P(O^iPr)_2]_3$ **39c**	2.736–2.742	80.34–97.65	3.533	–	[75]
$Ph_3Ge\{Se(Se)P(OEt)_2\}$ **40a**	2.405		–	–	[76]
$Ph_3Sn\{Se(Se)P(OEt)_2\}$ **41a**	2.570		–	–	[76]
$Ph_3Sn\{Se(Se)P(O^nPr)_2\}$ **41b**	2.573		–	–	[76]
$Ph_3Pb\{Se(Se)P(OEt)_2\}$ **42a**	2.658		–	–	[76]
$[Pb_2\{Se_2P(OMe)Ph\}_4]$ **44a**	2.830–3.269	72.18	–	–	[19]
$[Pb\{Se_2P(OEt)Ph\}_2]$ **44b**	2.925–3.224	75.22	–	–	[19]
$Sb\{Se_2P(O^iPr)_2\}_3$ **45c**	2.771–2.917	77.19	3.885		[49]
$Bi\{Se_2P(O^nPr)_2\}_3$ **46b**	2.902–2.908	76.14	3.795		[49]

I) and the non-coordinated, $Ph_2PSe_2^-$ anion links to the central polymeric core, via pairs of O–H···Se hydrogen bonds (Fig. 1). The Na–Se bond, 2.984 Å, is long.

An attempt to grow crystals of $Na[(Ph)(Pr^iO)PSe_2]$ led to hydrolytic degradation and formed the product $[(Ph)\{O^iPr\}PSeONa]_4(H_2O)_4$ [19]. Four Na atoms and four O atoms from ligand (one Se replaced by O) form a cubane with each Na also bonded to terminal H_2O ligand. Another interesting feature involves the O atom of each isopropyl group which is also coordinating to the adjacent Na atom.

The dimeric potassium complex $[K_2(Se_2PPh_2)_2(thf)_4]$ **3**, was obtained by reaction of potassium diphenylphosphide with two equiv. of gray selenium powder in thf [42]. The geometry around each potassium center with KSe_4O_2 core is distorted octahedral. The ligand adopts a μ_2-η^2, η^2 coordination mode (mode **IV**). ^{31}P NMR showed a single peak indicating equivalent chemical environments in solution. The air and moisture sensitive compound **3** is used to prepare metal complexes [42].

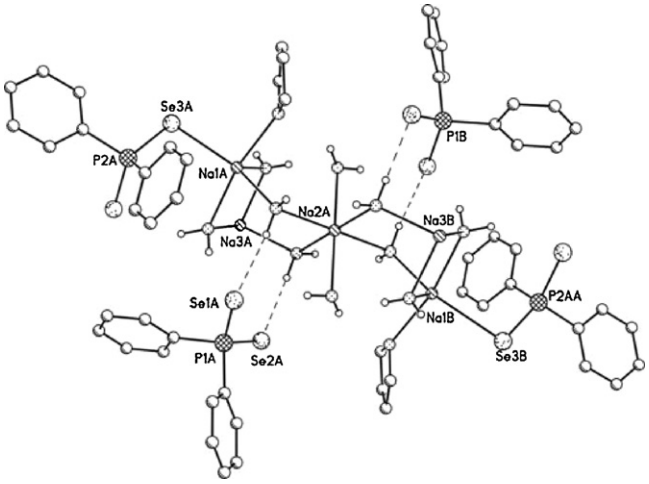

Fig. 1. Hydrogen bonded $Ph_2PSe_2^-$ anions (**2**) (adapted from Ref. [43]).

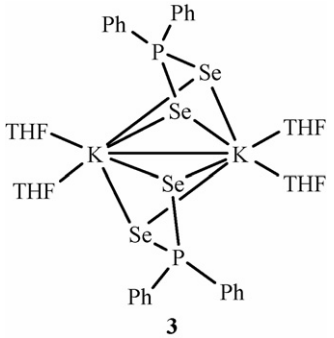

3

Reaction of $CyPH_2$ with *n*-BuLi and gray Se in tmeda base yielded a lithium complex $[CyPSe_3Li_2(tmeda)_2]$ **4** [40]. Each Li is coordinated by two Se atoms. All three Se atoms are coordinating and the ligand is acting as a tridentate, bridging ligand (mode **VII**). The ^{31}P NMR spectrum showed only one set of ^{77}Se satellites even at low temperature, however.

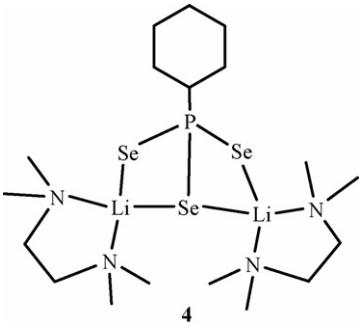

4

3.2. Group 4–6 elements (Ti, V, Cr, Mo)

Cyclopentadienyltitanium(IV) forms $Cp_2Ti(\eta^2\text{-}Se_2PPh_2)$ (**5**), and $Cp_2Ti(\eta^2\text{-}Se_2PCy_2)$ complexes with dsepi ligand via a series of different routes [44]. For example, allowing $Cp_2Ti(SePR_2)$ to stand in thf solution led to complete conversion to $Cp_2Ti(Se_2PR_2)$ (R = Ph, Cy). Other methods used are: from $(Cp_2TiCl)_2$ and $LiSePR_2$ in thf-hexane $(Cp_2TiCl)_2$ and $LiSe_2PR_2$, and by photolysis of $Cp_2Ti(CO)_2$ solution in thf containing one equivalent of $HSePR_2$. The structure of complex **5** shows chelation via Se, Se donor atoms of the Ph_2PSe_2 ligand with unequal Ti–Se bonds. It is ESR active with $g = 1.980$, which reveals rhombic environments around the metal center. Vanadium(III), vanadium(IV) and chromium(III) have formed paramagnetic octahedral complexes, $V(Se_2PEt_2)_3$ [45,46], $VO[Se_2P(OPr^i)_2]_2{\cdot}L$ (L = py, DMF, etc.) [48], $[CrL_3]$ {L = Se_2PEt_2 [47], $Se_2P(OEt)_2$ [1,3]}.

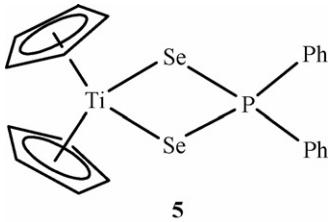

5

Oxidative decarbonylation of $Mo(CO)_6$ with $[(Pr^iO)_2P(Se)\text{-}Se\text{-}]_2$ yielded two clusters: mixed-valent ($Mo^{III/IV}$) dark brown $[Mo_4(\mu_3\text{-}Se)_4\{Se_2P(O^iPr)_2\}_6]$ **6** and orange $[Mo_3(\mu_3\text{-}Se)(\mu_2\text{-}Se_2)_3\{Se_2P(O^iPr)_2\}_3][Se_2P(O^iPr)_2]$, which subsequently abstracted a chloride from CH_2Cl_2 and formed $[Mo_3(\mu_3\text{-}Se)(\mu\text{-}Se_2)_3\{Se_2P(OPr^i)_2\}_3](Cl)$ **7** [49]. A related Mo_3 cluster $[Mo_3(\mu_3\text{-}Se)(\mu_2\text{-}Se_2)_3\{Se_2P(OEt)_2\}_3]Br$, **8** with ethoxyl substituents at P atom was prepared by the replacement of bromides with $(EtO)_2PSe_2^-$ in the trimolybdenum cluster $[Mo_3(\mu_3\text{-}Se)(\mu_2\text{-}Se_2)_3Br_6]^{2-}$ [50]. Cluster **6** has a Mo_4Se_4 central cubane-like core formed by triply bridging μ_3-Se atoms, and surrounded by four chelating and two bridging dsep ligands (Fig. 2). Thus each Mo atom is bonded to two Se atoms from one chelating dsep ligand, one Se from bridging dsep and

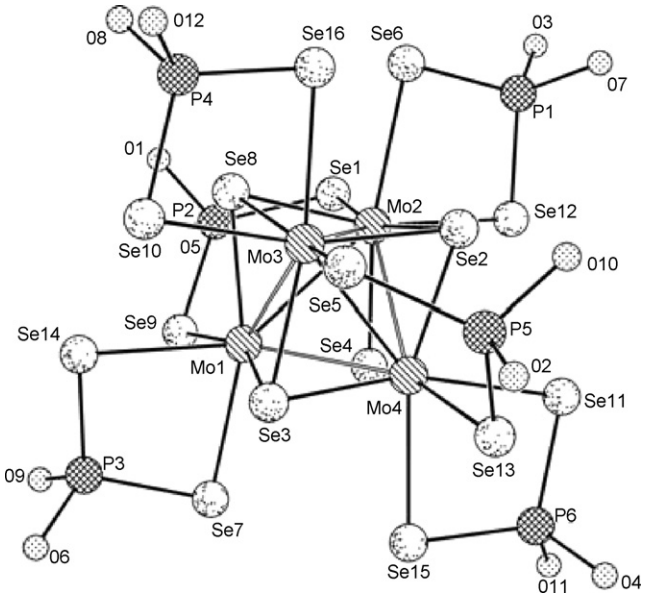

Fig. 2. Structure of cluster $[Mo_4(\mu_3\text{-}Se)_4\{Se_2P(O^iPr)_2\}_6]$ **6** (adapted from Ref. [49]).

to three different triply bridging μ_3-Se atoms. There are six Mo–Mo bonds with unequal distances. NMR (^{31}P and ^{77}Se) spectra reveal that the cluster is stable in the solution state. In its CV it shows one quasi-reversible one-electron oxidation wave (at 0.67 V versus AgCl/Ag) corresponding to the formation of the $[Mo_4Se_4](7+)$ and two quasi-reversible one-electron reduction waves (at −0.23, and −1.09 V versus AgCl/Ag), suggesting the formation of $[Mo_4Se_4](5+)$ and $[Mo_4Se_4](4+)$ cores.

Both cluster cations $[Mo_3(\mu_3\text{-}Se)(\mu\text{-}Se_2)_3\{Se_2P(O^iPr)_2\}_3](Cl)$ **7** [49], and $[Mo_3(\mu_3\text{-}Se)(\mu_2\text{-}Se_2)_3\{Se_2P(OEt)_2\}_3]Br$ **8** [50] have equivalent structures with three chelating dsep ligands, three $\mu\text{-}Se_2^{2-}$ bridges, and one μ_3-Se (face capping) atom (Fig. 3). The Mo–Se bonds vary in the order: $Mo\text{–}Se_{(central)} < Mo\text{–}Se_{(axial)} < Mo\text{–}Se_{(equatorial)} < Mo\text{–}Se_{(dsep)}$.

In the packing diagram the cluster **7** shows long-range Se···Se and Se···Cl interactions (Fig. 3). The chloride ion displays an interaction with three electrophilic axial Se atoms: Se1, Se3 and Se5 and one equatorial Se6 atom. The μ_3-Se atom exhibits an interaction with Se1 atom (axial), and finally, one Se atom of one dsep ligand of one Mo_3 unit interacts with Se5 atom (axial) of second Mo_3 unit and one Se atom of dsep ligand of this second unit. The Se···Se interactions lie in the range, 3.610–3.699 Å, while Cl···Se interactions lie in the range, 2.787–3.050 Å, which are less than the sum of van der Waals radii {4.0 Å, Se, Se; 3.70 Å Cl, Se}. NMR of clusters **7** and **8** revealed that the cluster cations are intact in the solution state.

3.3. Group 8–10 elements (Ru, Co–Ir, Ni–Pt)

Pentamethylcyclopendadienylruthenium(IV) with dsepi ligand formed a complex $[Cp^*Ru\{\eta^2\text{-}Se_2P^iPr_2\}\{\eta^2\text{-}SeP^iPr_2)\}](PF_6)$ **9** ($Cp^* = C_5Me_5$), by the reaction of $[Cp^*Ru(CH_3CN)_3](PF_6)$ with $HN[SeP^iPr_2]_2$ [52]. The formation of $Se_2P^iPr_2^-$ ligand probably involves initially P–N bond cleav-

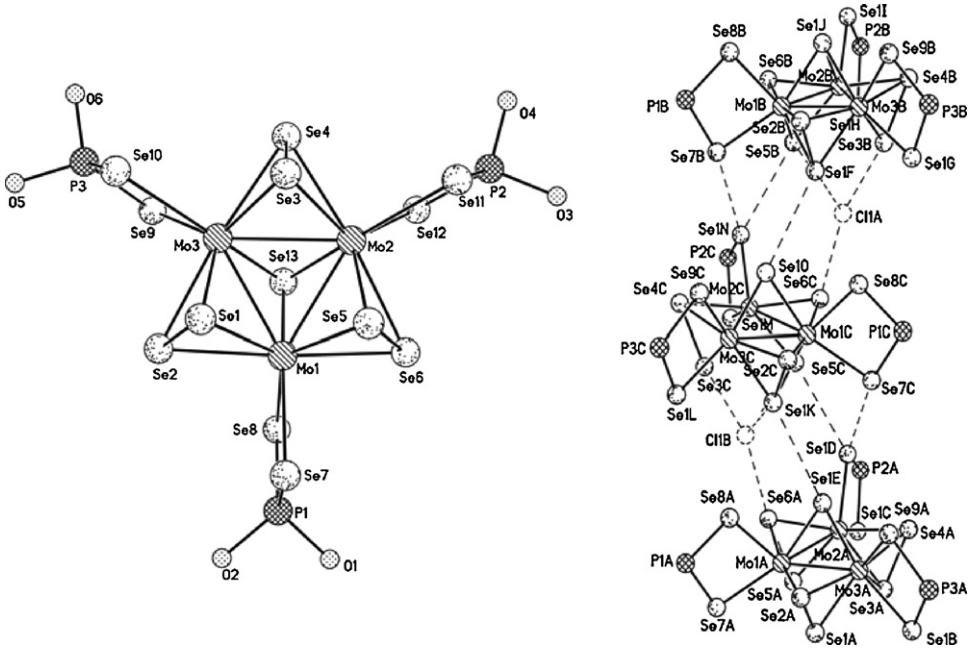

Fig. 3. Structure of cation $[Mo_3(\mu_3\text{-Se})(\mu\text{-Se}_2)_3\{Se_2P(O^iPr)_2\}_3]^+$ **7** (left) and its packing diagram displaying Se···Se and Se···Cl interactions (right) (adapted from Ref. [49]).

age to form $SeP^iPr_2^-$, then transfer of Se atom extruded from $HN[SeP^iPr_2]_2$ to the latter anion. The observed, η^2-SeP^iPr_2 fragment in **9** is unusual for a selenophosphinato moiety. Compound **9** adopts a four legged piano stool structure. As expected, the $SeP^iPr_2^-$ showed ^{31}P NMR chemical shift at lower field {δ 116.1 ppm) versus 5.5 ppm for $Se_2P^iPr_2^-$ ($^3J_{P-P} = 5.5$ Hz}.

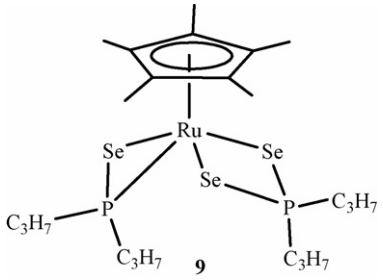

9

Other dsepi complexes are, $M(Se_2PPh_2)_2$ for M = Co, Ni [53,54]. The magnetic moment (μ, 4.75 BM) and electronic absorption spectra support the tetrahedral structure for $Co(Se_2PPh_2)_2$, and X-ray diffraction study confirmed the square planar structure for diamagnetic, $Ni(Se_2PPh_2)_2$ **10** [54]. The inner sphere oxidation of $Ni(PPh_2)\cdot PPh_2H$ with elemental Se also yielded **10** [55]. The dsep ligand formed octahedral complexes, $M[Se_2P(OEt)_2]_3$ for M = Co, Rh, and Ir [3,4], and a square planar compound, $Ni[Se_2P(OEt)_2]_2$ **11** [56]. Reaction of nickel(II) chloride with two moles of dsepo ligand, $Ph(MeO)PSe_2^-$ yielded the complex $[Ni\{Se_2P(OMe)Ph\}_2]$ **12** [19]. The nickel atom resides on a crystallographic inversion center and is coordinated by four Se atoms in a square planar arrangement with symmetric $NiSe_2P$ rings. This structure is similar to structures **10–11** as discussed above. NMR (^{31}P and ^{77}Se) spectra are consistent with the solid state structure and the structure is stable in the solution state.

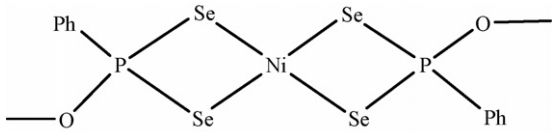

12

Compounds of the type, $Pd[Se_2P(OR)_2]_2$ (**13**, R = Et, Pr, ^{i}Pr), were prepared from the stoichiometric reaction of $Pd(CH_3CN)_2Cl_2$ and $NH_4Se_2P(OR)_2$ in CH_2Cl_2 [49]. A typical square planar complex, whose packing diagram displays intramolecular, secondary Se···Se interactions to form a single chain, also has unequal Pd–Se bonds (Fig. 4).

The reaction of *cis*-$PtCl_2$(dppe) with $Ph_2P_2Se_4$ in thf solvent or liquid ammonia gave the square planar complex, *cis*-$Pt\{Se_2(Se)PPh\}$(dppe) **14** containing the tsepo ligand [18]. Other tsepo complexes are: *cis*-$Pt\{Se_2(Se)PPh\}(PR_3)_2$ (R = Et, Ph_2Me, $PhMe_2$). Complex **14** has both chelating dppe, and $PhPSe_3^{2-}$ with unequal P–Se bonds. The dihedral angle between planes of $PtSe_2$ and PSe_2 is 13.2°, and the *trans* annular Se···Se distance is 3.34 Å. ^{31}P NMR data showed that complexes exist in solution and do not dissociate, but are air and moisture sensitive. For example, when *cis*-$Pt\{Se_2(Se)PPh\}(PMe_2Ph)_2$ was exposed to air in $CDCl_3$ solution, the terminal Se atom was replaced by O atom forming *cis*-$Pt\{Se_2(O)PPh\}(PMe_2Ph)_2$ [18].

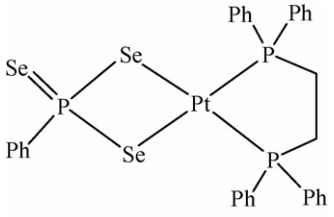

14

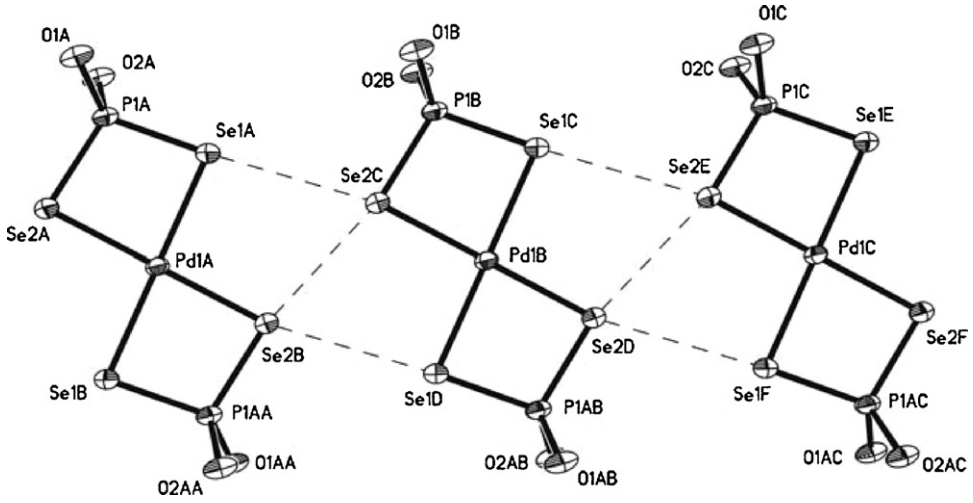

Fig. 4. Secondary Se···Se interactions revealed from the packing diagram of **13**.

3.4. Group 11 elements (Cu, Ag)

Since 1998 it has been known that diselenophosphates have yielded a wide variety of compounds with copper(I) and silver(I) [16,35]. Previously there were only preliminary reports on the formation of Cu^I and Ag^I complexes, $M[Se_2P(OEt)_2]$ ($M = Cu^I$, Ag^I) [4], $[Cu(Se_2PPh_2)]$ [53] and $Cu[Se_2P(OR)_2]_2$ (R = Et, ^{i}Pr) (ESR active) [5,57], and none of these were structurally characterized. The work is further split into two parts based on the metal.

3.4.1. Copper

Copper clusters with nuclearities ranging from 4, 8, 11 to 12 are depicted in Eqs. (1)–(7). Using different reaction routes, one or more types of clusters were formed. When the solvent was diethyl ether, either Se-centered cluster **15c** (Eq. (1)) or tetranuclear cluster **23** (Eq. (7)) were formed in the absence of halides. When chloride ion was present in ether medium, both chloride-centered **16a–c** and Se-centered *15a*, **15b–c** clusters were formed (Eq. (3)). The presence of iodide did not form iodide-centered cubanes, rather clusters with $Cu_{11}(\mu_9\text{-Se})(\mu_3\text{-I})_3$ cores were formed apart from Se-centered clusters (Eq. (2)). When ether was replaced by CH_2Br_2, bromide-centered clusters **17a**, *17b*, **17c**, Se-centered clusters *15a*, **15b–c**, and clusters with $Cu_{11}(\mu_9\text{-Se})(\mu_3\text{-Br})_3$ cores were formed (Eq. (4)). Eq. (5) shows that using a different molar ratio of reactants, undecanuclear copper clusters were not formed. Eq. (6) shows the formation of unusual dodecanuclear copper clusters containing an ethane-like hexaselenodiphosphate **20a**, **c**, apart from *15a* and **15c**. Thus with the exception of the tetrahedral cluster **23** which appears as an intermediate in the formation of octanuclear or other clusters of higher nuclearities, the rupture of P–Se bonds does occur in order to stabilize a cluster. The discussion in the subsequent pages follows the classification based on the nuclearity of a cluster (bold number shows the complex whose X-ray structure is known):

$$Cu^+ + \underset{[16]}{2(^iPrO)_2PSe_2^-} \xrightarrow{Et_2O} \{Cu_8(\mu_8\text{-Se})[(Se_2P(O^iPr)_2]_6\}\ \mathbf{15c} \quad (1)$$

$$2Cu^+ + \underset{[59]}{3(RO)_2PSe_2^-} + 2(Bu_4N)I \xrightarrow{Et_2O} \begin{cases} \{Cu_8(\mu_8\text{-Se})[(Se_2P(OR)_2]_6\} & R = {}^n\text{Pr}, {}^i\text{Pr}, \mathbf{15b\text{-}c} \\ + \\ \{Cu_{11}(\mu_9\text{-Se})(\mu_3\text{-I})_3[(Se_2P(OR)_2]_6\} & \\ R = {}^n\text{Pr}\ \textit{19b},\ {}^i\text{Pr}\ \mathbf{19c} & \end{cases} \quad (2)$$

$$4Cu^+ + \underset{[63]}{3(RO)_2PSe_2^-} + 1(Bu_4N)Cl \xrightarrow{Et_2O} \begin{cases} [Cu_8(\mu_8\text{-Cl})[(Se_2P(OR)_2]_6](PF_6) + & \\ R = \text{Et}, {}^n\text{Pr}, {}^i\text{Pr}, \mathbf{16a\text{-}c} & \\ \{Cu_8(\mu_8\text{-Se})[(Se_2P(OR)_2]_6\} \quad R = \text{Et}, \textit{15a}; \mathbf{15b, 15c} & \end{cases} \quad (3)$$

$$2Cu^+ + \underset{[36,60]}{3(RO)_2PSe_2^-} + 2(Bu_4N)Br \xrightarrow{CH_2Br_2} \begin{cases} \{Cu_8(\mu_8\text{-Se})[(Se_2P(OR)_2]_6\} \quad (\textit{15a}, \mathbf{15b, 15c}) + & \\ [Cu_8(\mu_8\text{-Br})[(Se_2P(OR)_2]_6](PF_6) + & \\ R = \text{Et}\ \mathbf{17a}, {}^n\text{Pr}\ \textit{17b}, {}^i\text{Pr}\ \mathbf{17c} & \\ \{Cu_{11}(\mu_9\text{-Se})(\mu_3\text{-Br})_3[(Se_2P(OR)_2]_6\} & \\ R = \text{Et}\ \textit{18a}, {}^n\text{Pr}\ \textit{18b}, {}^i\text{Pr}\ \mathbf{18c} & \end{cases} \quad (4)$$

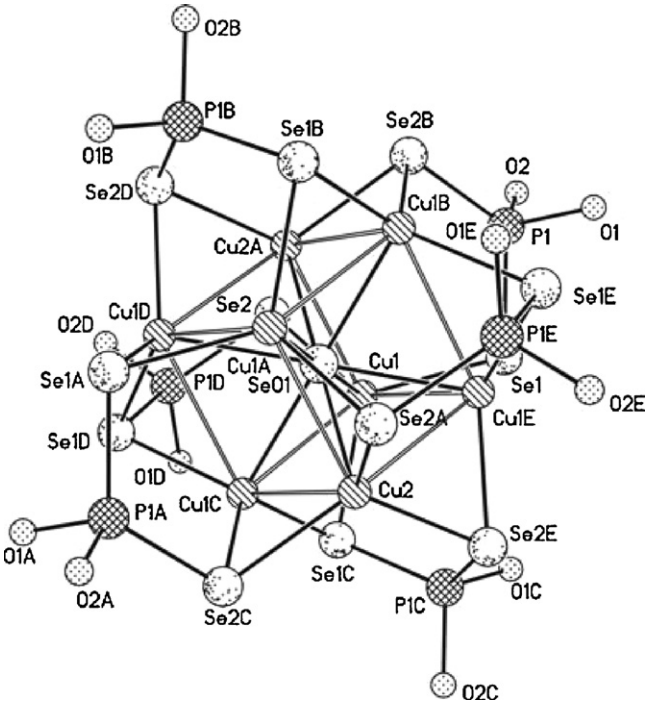

Fig. 5. Structure of $[Cu_8(\mu_8\text{-Se})\{Se_2P(O^nPr)_2\}_6]$ **15b** (adapted from Ref. [59]).

$$4Cu^+ + 3(RO)_2PSe_2^- + 1(Bu_4N)Br \xrightarrow{CH_2Br_2} \begin{cases} \{Cu_8(\mu_8\text{-Se})[(Se_2P(OR)_2]_6\} \quad (\textit{15a}, \textbf{15b}, \textbf{15c}) + \\ [Cu_8(\mu_8\text{-Br})[(Se_2P(OR)_2]_6](PF_6) \\ \quad R = Et\ \textbf{17a}, {}^nPr\ \textit{17b}, {}^iPr\ \textbf{17c} \end{cases} \quad (5)$$

[36,60]

$$Cu^+ + 3(RO)_2PSe_2^- \xrightarrow{CH_2Cl_2} \begin{cases} \{Cu_8(\mu_8\text{-Se})[(Se_2P(OR)_2]_6\} + \\ \quad \textit{15a}, \textbf{15c} \\ \{Cu_{12}(P_2Se_6))[Se_2P(OR)_2]_8\} \\ \quad R = Et\ \textbf{20a}, {}^iPr\ \textbf{20c} \end{cases} \quad (6)$$

[37]

$$Cu^+ + ({}^iPrO)_2PSe_2^- \xrightarrow{Et_2O} \{Cu_4[(Se_2P(O^iPr)_2]_4\}\ \textbf{23} \quad (7)$$

[58]

3.4.1.1. Selenide-centered octanuclear clusters. Three octanuclear, Se-centered clusters $\{Cu_8(\mu_8\text{-Se})[Se_2P(OR)_2]_6\}$ for R = Et (15a), ^{n}Pr (**15b**) [60], ^{i}Pr (**15c**) [16] are reported, and structures of **15c** and 15**b** are established by X-ray crystallography. Both **15b** and **15c** are isostructural and have an interstitial selenide ion (Se^{2-}) (Fig. 5). The copper atoms are arranged at the corners of an almost regular cubane, and each dsep ligand exhibits a "tetrametallic tetraconnective" (μ_2, μ_2; mode **VI**) connection pattern [6] and occupies the square face of a cube. Each copper atom of the cube is coordinated to three Se atoms of three different bridging dsep ligands, and the geometry around each copper atom is distorted trigonal planar. Overall due to the lack of four-fold rotational axis, the molecules **15b–c** have an idealized T_h point group symmetry. The central selenide, and 12 Se atoms of the dsep ligands, form a body-centered icosahedron, and structures of this type are known for the Fenske's clusters, $Cu_{20}(\mu_8\text{-Se})Se_{12}(PEt_3)_{12}$ [61] and $Cu_{26}Se_{13}(PEt_2Ph)_{14}$ [62]. The Cu···Cu distances in **15b–c** (2.899–2.928 Å) and Cu–μ_8Se distances (2.504–2.577 Å) are only slightly shorter than those observed in the Fenske's clusters (Cu···Cu, 3.008 Å, Cu–μ_8Se, 2.605 Å) [61]. The bulky isopropoxyl groups at the P atom appear to have virtually no effect on Cu–Se bonds and Se···Se bite distances (3.776, **15b**; 3.784 Å, **15c**). ^{31}P NMR and ^{77}Se spectra of **15b–c**, typically a singlet flanked with a set of satellites for ^{31}P NMR and a doublet for ^{77}Se NMR, reveal that the six dsep ligands are equivalent in solution. The selenide in the center was also detected by ^{77}Se NMR spectroscopy (**15b**, −1147.4; **15c**, −1172.6 ppm) [59].

3.4.1.2. Halogen-centered octanuclear clusters. Only the chloride and bromide-centered octanuclear clusters $[Cu_8(\mu_8\text{-X})\{Se_2P(OR)_2\}_6](PF_6)$ (X = Cl, R = Et, ^{n}Pr, ^{i}Pr, **16a–c** [63]; X = Br, R = Et, ^{n}Pr, ^{i}Pr, **17a** [60], *17b*, **17c** [36]) have been reported. The chloride and bromide clusters **16a–c**, **17a**, and **17c** are structurally similar. Eight copper ions are at the corners of a cube and are linked to Se donor atoms of six dsep ligands, adopting the same coordination pattern as that in Se-centered clusters, **15b–c**. Each copper ion is bonded strongly to the central μ_8-X (X = Cl, Br) ions, with PF_6^- as a non-coordinating anion (Fig. 6).

The geometry around each Cu ion bonded to three selenium atoms is trigonal planar. The average Cu···Cu distances vary in the order: Se-centered clusters (2.859–2.974 Å, **15**) < Cl-centered clusters (3.13–3.15 Å, **16**) < Br-centered clusters (3.18–3.19 Å, **17**). While the analogous dithiophosphate, halide-centered clusters showed Cu···Cu distances, 3.18–3.44 Å [9,10], the sulfur-centered, dithiophosphate clusters showed in the range 2.95–3.00 Å [21,22]. The Se···Se bite distances also varied in the order: **15** (3.780 Å) < **16** (3.801–3.811 Å) < **17** (3.807–3.823 Å). Furthermore, while Cu–(μ_2-Se) bond distances are nearly the same in halide-centered clusters (2.365–2.408 Å, **16**; 2.360–2.404 Å, **17**) but are slightly shorter than those observed in Se-centered clusters **15** (2.447–2.461 Å), NMR data (^{31}P, ^{77}Se) suggest that all dsep ligands in clusters **16–17** remain equivalent in solution.

3.4.1.3. Selenide-centered undecanuclear was clusters. The reaction depicted in Eq. (2) originally designed to prepare iodide-centered cubic clusters analogous to chloride or bromide-centered clusters (**16–17**) by using Bu_4NI; however, it resulted in the formation of nonacoordinated (μ_9-Se) selenide-centered copper clusters with three capping iodo ligands, $Cu_{11}(\mu_9\text{-Se})(\mu_3\text{-I})_3[Se_2P(OR)_2]_6$ {R = ^{n}Pr *19b*, ^{i}Pr **19c**} [59]. Similarly Eq. (4) shows the formation of analogous bromide-bridged, undecanuclear copper clusters, $Cu_{11}(\mu_9\text{-Se})(\mu_3\text{-Br})_3[Se_2P(OR)_2]_6$ (R = Et *18a*; ^{n}Pr *18b*; ^{i}Pr, **18c**) [36,60]. When a lesser amount of Bu_4NBr was used, it did not form clusters **18a–c**, rather clusters **15a–c**, and **17a–c** were formed. The direct reaction of Se-centered cluster, **15c**, with

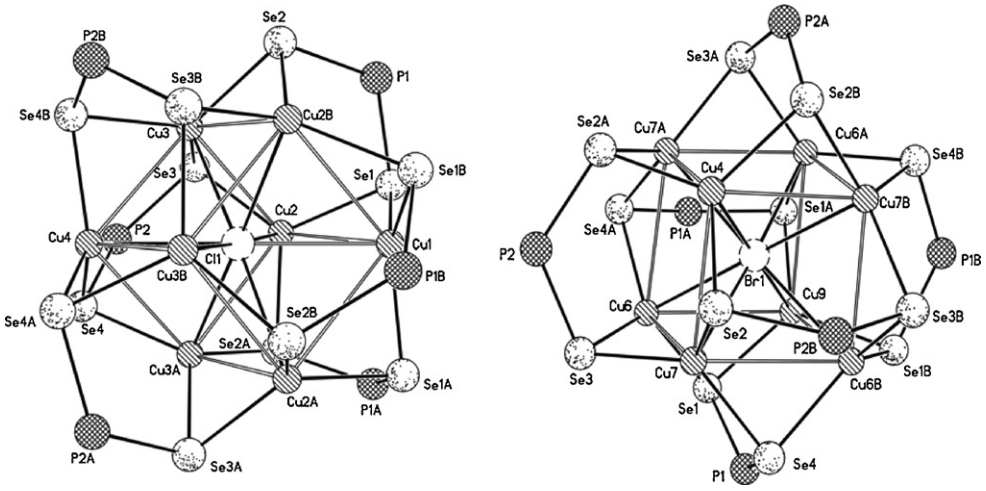

Fig. 6. Structure of cluster cations $[Cu_8(\mu_8\text{-Cl})\{Se_2P(OEt)_2\}_6]^+$ **16a** (left) and $[Cu_8(\mu_8\text{-Br})\{Se_2P(OEt)_2\}_6]^+$ **17a** (right) (adapted from Refs. [60,63]).

excess amount of Bu_4NBr or Bu_4NI did not form **19c** [59] or **18c** [36]. Thus the cluster nuclearity does not increase from 8 to 11 in the presence of iodide or bromide ions in solution. Chloride did not form the analogous Cu_{11} clusters. X-ray crystallography reveals that clusters **18c** and **19c** are examples possessing not only a 3,3,4,4,4-pentacapped trigonal prismatic copper framework (Cu_{11}), but also a nonacoordinated bridging selenido ligand in a tricapped prismatic geometry (Fig. 7). The $Cu_{11}Se$ core having an idealized D_{3h} point group symmetry is further stabilized by three bromide (or iodide) and six dsep ligands (Fig. 7).

There exist a total of nine Cu_4 butterflies where the wing-tip positions are represented by the five capping copper atoms with each edge and height of the trigonal prism being the hinges. Those Cu_4 butterflies comprising a copper atom on the C_3 axis are each connected by a dsep ligand in a μ_2, μ_2-coordination pattern. The remaining three butterflies where hinge positions are the heights of the prism, are each occupied by a triply bridging bromide (or iodide) atom over an alternating set of three of the six triangular faces. Significantly, shorter Cu···Cu bond distances are revealed between the capping atoms and the prism, viz., 2.787(2)–3.154(2) Å, slightly longer than the sum of the van der Waals radii of Cu (2.80 Å) [64,65]. Both Cu(1) and Cu(2), each capping the triangular face of the prism, as well as encapsulated Se are located on the pseudo three-fold axis. Overall, owing to the existence of triply bridging halides, the D_{3h} symmetry observed in Fig. 14 is lowered to C_{3h} symmetry. Multinuclear NMR (^1H, ^{31}P and ^{77}Se) experiments unequivocally support the view that the local symmetry of C_{3h} is retained in solution for clusters **18–19**. The ^{77}Se NMR resonance frequencies for the (μ_9-Se) atom occur at high field {δ_{Se}, ca. −1190 to 1220 ppm, **18**, **19**}. Molecular orbital calculations at the B3LYP level of the density functional theory for the study of Cu–(μ_9-Se) interactions in clusters **18c** and **19c** have shown that the formal bond order of each Cu–(μ_9-Se) bond is slightly smaller than half of those calculated for the terminal Cu–(μ_2-Se) bonds.

3.4.1.4. Dodecanuclear copper cluster. Cluster $[Cu_{12}(P_2Se_6)[Se_2P(OEt)_2]_8]$ **20a**, is the first example of a discrete, neutral molecule containing an ethane-like hexaselenodiphosphate(IV), $P_2Se_6^{4-}$, bridging group; the coexistence of P^{4+} and P^{5+} centers in the same compound is also rare (Fig. 15)

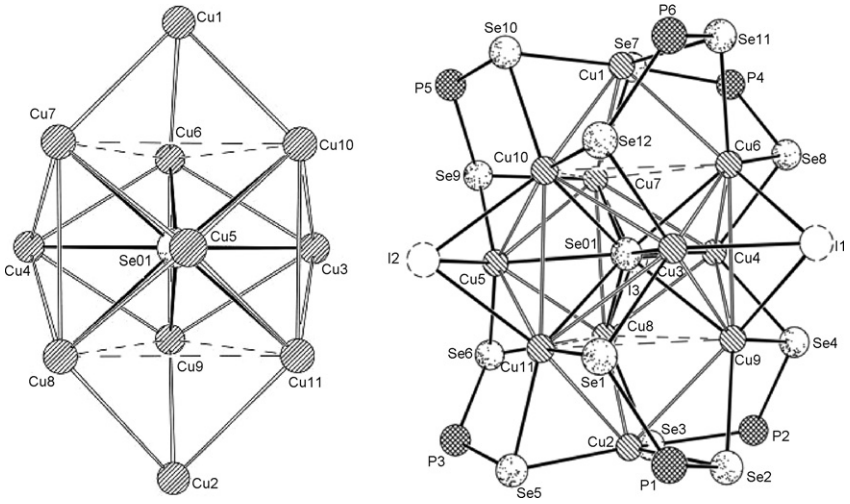

Fig. 7. $Cu_{11}(\mu_9\text{-Se})$ core in **19c** (left); structure of $Cu_{11}(\mu_9\text{-Se})(\mu_3\text{-I})_3[Se_2P(O^iPr)_2]_6$ **19c** with isopropoxyl groups omitted (right) (adapted from Ref. [59]).

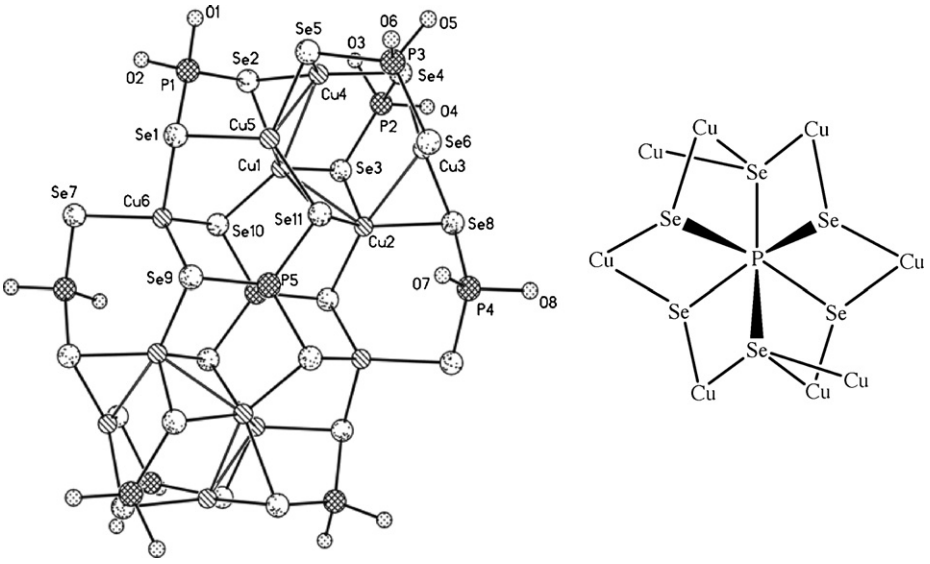

Fig. 8. Structure of $[Cu_{12}(P_2Se_6)[Se_2P(OEt)_2]_8]$ **20a** with ethyl groups omitted (left) and its central core $P_2Se_6^{4-}$ (right) (adapted from Ref. [37]).

[37]. Dodecanuclear copper cluster is stabilized by eight dsep ligands and a $P_2Se_6^{4-}$ ion which is located in the center of the cluster and has ethane-like geometry in a staggered conformation. With a center of symmetry at the midpoint of the P–P bond, each 'PSe_3' moiety of the $P_2Se_6^{4-}$ ligand consists of one μ_3-Se atom and two μ_2-Se atom that bridge seven Cu atoms. Overall the $P_2Se_6^{4-}$ ligand adopts an unprecedented μ_8:η^3:η^2:η^2:η^3:η^2:η^2 coordination mode (Fig. 8). The four outer copper atoms are additionally connected to the eight inner copper atoms by eight dsep ligands. The dsep ligands exhibit two distinct bridging modes. Four of them adopt a trimetallic triconnective (mode **V**) and the rest show μ_2, μ_2 coordination patterns. The structure of $[Cu_{12}(P_2Se_6)[Se_2P(O^iPr)_2]_8]$ **20c** is almost identical to **20a**. Variable temperature ^{31}P NMR studies showed that $Cu_{12}(P_2Se_6)$ core remains intact in solution, while the peripheral, eight dsep ligands are fluxional in solution, indicating the lability of Cu–Se bonds.

3.4.1.5. Ligand substitution in the cubic cluster. The reaction of $[Cu_8(\mu_8\text{-Se})\{Se_2P(O^nPr)_2\}_6]$ **15b** with $(NH_4)[S_2P(OEt)_2]$ formed $\{Cu_8(\mu_8\text{-Se})[S_2P(OEt)_2]_6\}_{0.54}\{Cu_6[S_2P(OEt)_2]_6\}_{0.46}$, which is a co-crystallized product of two independent clusters, $Cu_8(\mu_8\text{-Se})[S_2P(OEt)_2]_6$ **21** and $Cu_6[S_2P(OEt)_2]_6$ **22** (Fig. 9) [66]. The formation of **21** in the co-crystals shows that all the six dsep ligands in **15b** are replaced by $[S_2P(OEt)_2]^-$ and the formation of **22** shows the extrusion of selenium from the interior of the cube, probably as a Cu_2Se moiety, along with the substitution of dsep ligands by dithiophosphates. However, the exact mechanism for the formation of **22** is not clear. The $Cu_8(\mu_8$-Se) cubic core in **21** is larger in size than the metal core in **15b**, although the Se···Se bite distance of **15b** is larger than the S···S bite distances of 3.478 Å in **21**. The presence of central selenide in **21** is unequivocally confirmed by ^{77}Se NMR (δ, −976 ppm). The ^{31}P NMR showed lability of Cu–S bonds in solution and solid state MAS NMR showed two types of phosphorus nuclei

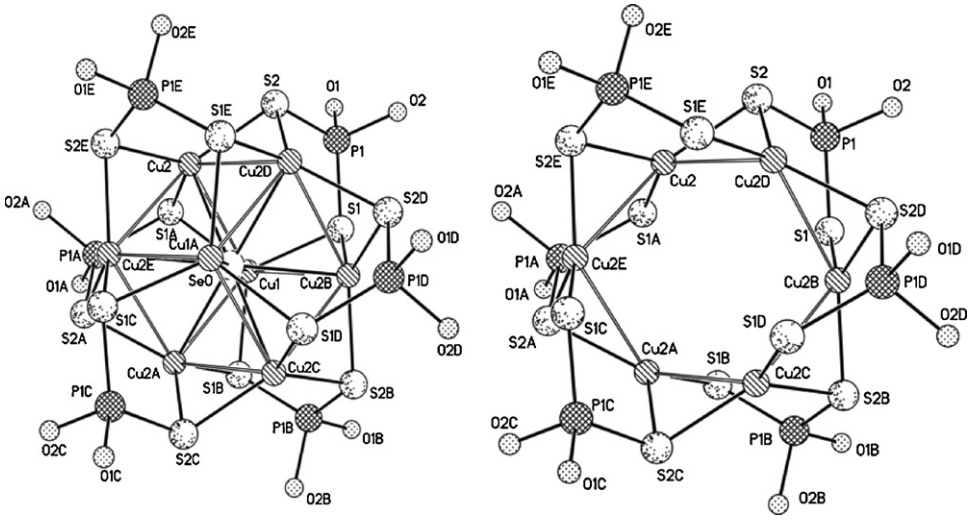

Fig. 9. Structures of $[Cu_8(\mu_8\text{-Se})\{S_2P(OEt)_2\}_6]$ **21** (left) and $Cu_6[S_2P(OEt)_2]_6$ **22** (right) (adapted from Ref. [66]).

in **21** (δ, 101.1 ppm) and **22** (δ, 100.7 ppm). In cluster **22**, each dtp ligand adopts μ_2, μ_1-coordination pattern. The cluster **21** is the first selenide-centered Cu^I_8 cube cluster surrounded by the dithiophosphato ligands. This co-crystallization phenomenon is rare in copper cluster chemistry. Molecular orbital calculations suggest that Cu–μ_8-Se interactions are not very strong and a half bond can be formally assigned to each Cu–μ_8-Se bond [66].

The Cu···Cu separation among cubic clusters, **15–17** and **21** varies in the order: clusters **15** < cluster **21** < clusters **16–17**. Hence it may be summarized as follows: a softer peripheral ligand with a soft atom at the center appears to favor closer metal–metal contacts. A more electronegative atom at the center of a cube or a more electronegative peripheral ligand favors longer metal–metal contacts. Furthermore, Cu···Cu contacts do not show cuprophilicity in **15–19** and **21** clusters; however, in dodecanuclear copper clusters, **20**, cuprophilicty was noted.

3.4.1.6. Tetranuclear cluster. The four copper atoms in $[Cu_4\{Se_2P(O^iPr)_2\}_4]$ **23**, each located at the vertex of a tetrahedron, are held together with four face-capped dsep ligands in a μ_2, μ_1-coordination pattern (mode **V**) to form a tetranuclear unit (Fig. 10). Each copper atom is trigonally coordinated to three selenium atoms from three dsep ligands. ^{31}P and ^{77}Se NMR suggest that all dsep ligands are equivalent in solution. Clusters **23** have been utilized as a single source precursor for the fabrication of non-stoichiometric, copper selenide ($Cu_{2-x}Se$) nanowires via a self-catalytic vapor–liquid–solid growth pathway [58]. Its formation is attributed to the easy cleavage of the P–Se bond of the dsep ligands.

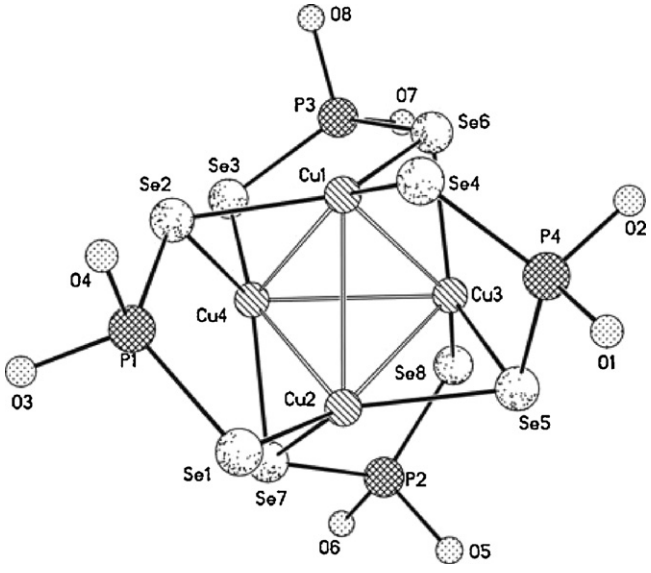

Fig. 10. Structure of $[Cu_4\{Se_2P(O^iPr)_2\}_4]$ **23** with isopropyl groups omitted (adapted from Ref. [49]).

3.4.2. Silver

Silver(I) forms various types of clusters with nuclearity ranging from hexanuclear, octanuclear, decanuclear, undecanuclear to polymeric (Eqs. (8)–(11)). In contrast, copper(I) did not form any polymeric species with the dsep ligands for no apparent reason. As in the case of copper, P–Se bond cleavage occurs during reactions and the Se atom gets transferred into the center of a polyhedron. The formation of halogen-centered octanuclear silver clusters appears more frequently, as are hexanuclear and decanuclear clusters vis-à-vis selenium-centered octanuclear copper clusters:

$$\underset{[35]}{Ag^+ + 2(RO)_2PSe_2^-} \xrightarrow[CH_2Cl_2]{R=^iPr} \underset{\mathbf{24}}{[Ag_8(\mu_8\text{-Se})\{Se_2P(O^iPr)_2\}_6]} + \underset{\mathbf{25}}{[Ag_6\{Se_2P(O^iPr)_2\}_6]} \quad (8)$$

$$4Ag^+ + 3(RO)_2PSe_2^- + 1Bu_4NX \xrightarrow[[67,68]]{CH_2X_2} \begin{cases} [Ag_8(\mu_8\text{-X})\{Se_2P(OR)_2\}_6](PF_6) \\ \quad X=Cl,\ R=Et,\ \mathbf{26a};\ {}^nPr,\ \mathbf{26b};\ {}^iPr,\ 26c \\ \quad X=Br,\ R=Et,\ \mathbf{27a};\ {}^nPr,\ \mathbf{27b};\ {}^iPr,\ 27c \\ + \\ [Ag_{10}(\mu_{10}\text{-Se})\{Se_2P(OR)_2\}_8] \\ \quad R=Et,\ \mathbf{28a};\ {}^nPr,\ 28b;\ {}^iPr,\ 28c \end{cases} \quad (9)$$

$$Ag^+ + (RO)_2PSe_2^- \xrightarrow[[38]]{Et_2O} \begin{cases} [Ag_{10}(\mu_{10}\text{-Se})\{Se_2P(OR)_2\}_8]\ (\mathbf{28a}, 28c) + \\ \{Ag[Se_2P(OR)_2]\}_n\ R=Et,\ 29a,\ n=\infty;\ {}^iPr,\ \mathbf{29c},\ n=6 \end{cases} \quad (10)$$

$$4Ag^+ + \underset{[69]}{3(RO)_2PSe_2^-} + Bu_4NI \xrightarrow{CH_2Cl_2} [Ag_{11}(\mu_9\text{-Se})(\mu_3\text{-I})_3\{(Se_2P(OR)_2\}_6],$$
$$R = Et,\ 30a;\ {}^iPr,\ \mathbf{30c};\ {}^2Bu,\ \mathbf{30d} \quad (11)$$

3.4.2.1. Selenide-centered octanuclear cluster. The selenide-centered octanuclear cluster, $\{Ag_8(\mu_8\text{-Se})[Se_2P(O^iPr)_2]_6\}$ **24** was formed as shown in Eq. (8), along with the hexanuclear $\{Ag_6[Se_2P(O^iPr)_2]_6\}$ cluster **25**, which shared a common $\{Ag_6[Se_2P(O^iPr)_2]_6\}$ unit and superimposed along the three-fold axis in the trigonal lattice [35]. The crystal structure showed equal occupancy of Ag_8 and Ag_6 clusters which were alternately distributed along the three-fold axis of the trigonal lattice. In the octanuclear cluster **24**, Ag atoms and dsep ligands are arranged in a manner (Fig. 11), similar to that in Cu_8 cluster **15c** [16]. The coordination environment around each Ag atom of the cube is very similar to that observed in cluster **15c**, aside from the interaction to the central selenide anion. Two different bond lengths, 2.714 and 2.868 Å, are observed between the central selenium atom and peripheral Ag atoms so that a slightly compressed cube

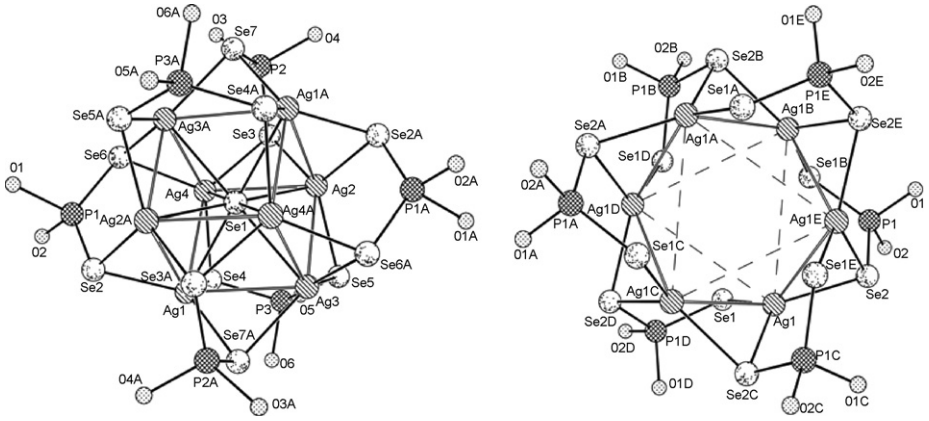

Fig. 11. Structures of $[Ag_8(\mu_8\text{-Se})\{Se_2P(O^iPr)_2\}_6]$ **24** (left) and $Ag_6[Se_2P(O^iPr)_2]_6$ **22** (right) (adapted from Ref. [35]).

is observed along the three-fold axis. This leads to a difference in Ag···Ag distances ranging from 3.180 to 3.358 Å, which are less than twice the sum of the van der Waals radius of Ag atom, 3.40 Å [64,65]. The Se···Se bite distance of 3.771 Å is comparable to that in clusters **15**. The central selenide and 12 Se atoms of six ligands also form a body-centered icosahedron, similar to that in clusters **15**.

Six silver atoms of **25** form a slightly compressed octahedron (Fig. 18). This octahedron consists of two uncapped equilateral triangles through which the three-fold axis passes, and six isosceles triangles in which each triangular face is capped by a dsep ligand in a trimetallic triconnective (μ_2, μ_1) coordination mode. Each Ag atom is coordinated to three Se atoms of three different dsep ligands with averaged Ag–Se bond distance of 2.621 Å. The variable temperature ^{31}P NMR study showed only one type of environments in the co-crystals in solution, and it is attributed to the high labilities of Ag–Se bonds.

3.4.2.2. Halogen-centered octanuclear clusters. Among the six, reported halogen-centered octanuclear clusters, $[Ag_8(\mu_8\text{-X})\{Se_2P(OR)_2\}_6](PF_6)$ (X = Cl, R = Et, ^{n}Pr, ^{i}Pr, **26a–b**, *26c*; **X** = Br, R = Et, ^{n}Pr, ^{i}Pr, **27a–b**, *27c*), four are structurally characterized [67,68]. A representative drawing of **27b** is depicted in Fig. 12. The general structure feature consists of a discrete cationic cluster in which eight silver ions are linked by six face-capped diselenophosphate ligands and a central μ_8-Cl or μ_8-Br ion with a non-coordinating PF_6^- anion. Silver atoms occupy the corners of the slightly distorted cube. Each dsep ligand exhibits a μ_2, μ_2-coordination pattern (mode **VI**), and occupies a square face of the cube in the same way as in the case of copper(I). Each Ag(I) is coordinated to three selenium atoms of three different ligands, and in addition, each Ag(I) interacts with the central halide ion. The coordination geometry around halide is close to cubic although some irregular Ag–X distances (Cl: 2.809–3.020 Å; Br: 2.865–3.072 Å) are observed.

The Ag···Ag distances are comparable among halide-centered silver clusters and the average Ag···Ag distance (3.37 Å) in **26–27** clusters is longer than the average 3.27 Å distance in the selenide cluster, **24**. These Ag···Ag distances are less than twice the sum of the van der Waals radius of Ag atom, 3.40 Å, an indicative of the existence of argentophilicity. The Se···Se distances (3.805–3.818 Å) are longer in halide-centered **26–27** clusters than those in Se-centered cluster **24**, and are comparable to those in copper clusters. The NMR data suggest that all the dsep ligands are equivalent in solution and the geometry of the compounds remains the same both in the solid and solution phase.

DFT calculations show weak bonding interactions between μ_8-X (X = Cl, Br) and Ag atoms [68]. Due to the higher electronegativity of Cl or Br versus Se, Ag–μ_8-X bonds are expected to be more ionic, while the Ag–μ_8-Se and Cu–μ_8-Se bonds are more covalent. The magnitude of the $Ag_8(\mu_8\text{-X})$ core expansion (0.10 Å in radius) from $Ag_8(\mu_8\text{-Cl})$ to $Ag_8(\mu_8\text{-Br})$ is smaller than the increase (0.15 Å) in size from Cl^- [$r(Cl^-) = 1.67$ Å] to Br^- [$r(Br^-) = 1.82$ Å] [51]. Therefore, the covalent interactions between Ag and μ_8-Br are stronger than that between Ag and μ_8-Cl. The magnitude of the $M_8(\mu_8\text{-Se})$ core expansion from $Cu_8(\mu_8\text{-Se})$ to $Ag_8(\mu_8\text{-Se})$ is in the range 0.21–0.35 Å in

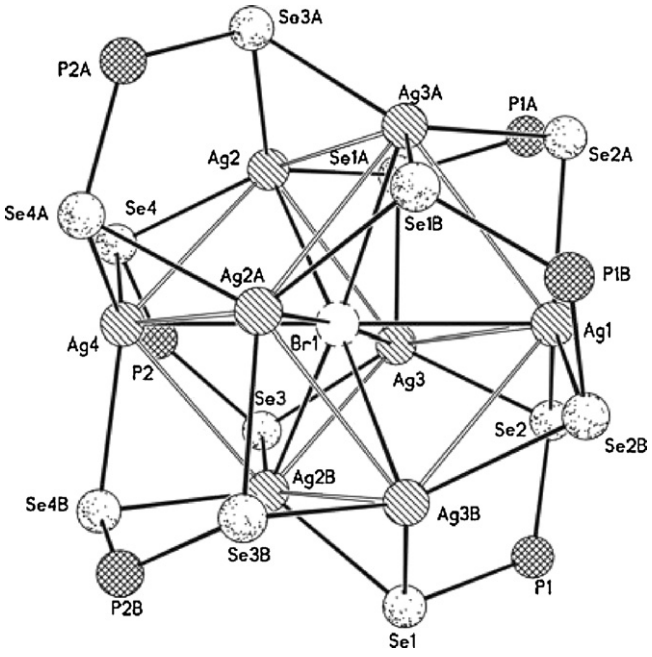

Fig. 12. Structure of the cation $[Ag_8(\mu_8\text{-Br})\{Se_2P(OEt)_2\}_6]^+$ **27a** with ethoxyl groups omitted (adapted from Ref. [68]).

radius, which is smaller than the increase (0.40 Å) in the size from Cu^+ [r(Cu^+) = 0.74 Å] to Ag^+[r(Ag^+) = 1.14 Å]. Again the Ag is expected to have more covalent interactions with the central Se.

3.4.2.3. Selenide-centered decanuclear clusters. Among the three reported, selenium-centered decanuclear silver clusters, $[Ag_{10}(\mu_{10}\text{-Se})\{Se_2P(OR)_2\}_8]$ (R = Et, **28a**, ^{n}Pr, *28b*, ^{i}Pr, *28c*) [38,68] (Eqs. (9) and (10)), the crystal structure is known only for **28a**. Fig. 13 shows the structure of Ag_{10} cluster. The coordination geometry around the central Se(1) atom can be best described as a distorted *cis*-bicapped trapezoidal prism, where two unequal trapezoidal planes are defined by Ag(1)–Ag(2)–Ag(6)–Ag(9) and Ag(3)–Ag(4)–Ag(10)–Ag(7) with Ag(5) and Ag(8) as capping atoms. The solution NMR study (^{31}P and ^{77}Se) did not show differences in chemical environments for dsep ligands. Only one signal flanked with a set of satellites in ^{31}P and a doublet in ^{77}Se NMR were observed and this further reveals the lability of Ag–Se bonds. The chemical shift of the central Se is at $\delta = -1396$ ppm.

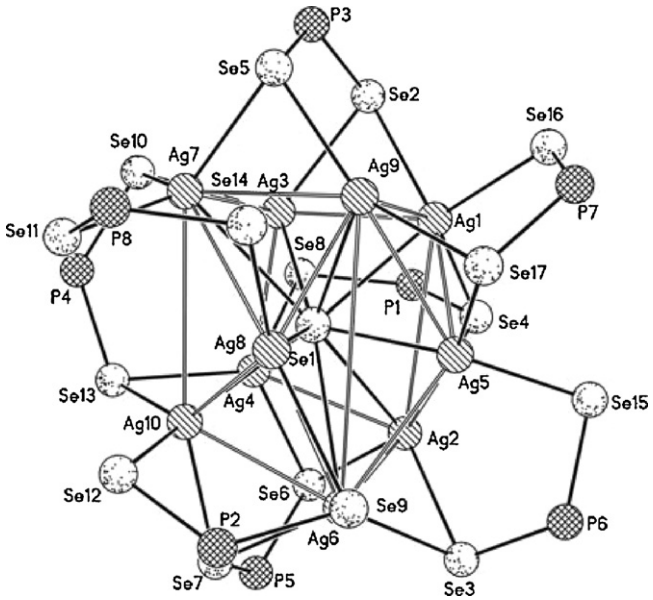

Fig. 13. Structure of $[Ag_{10}(\mu_{10}\text{-Se})\{Se_2P(OEt)_2\}_8]$ **28a** with ethoxyl groups omitted for clarity (adapted from Ref. [38]).

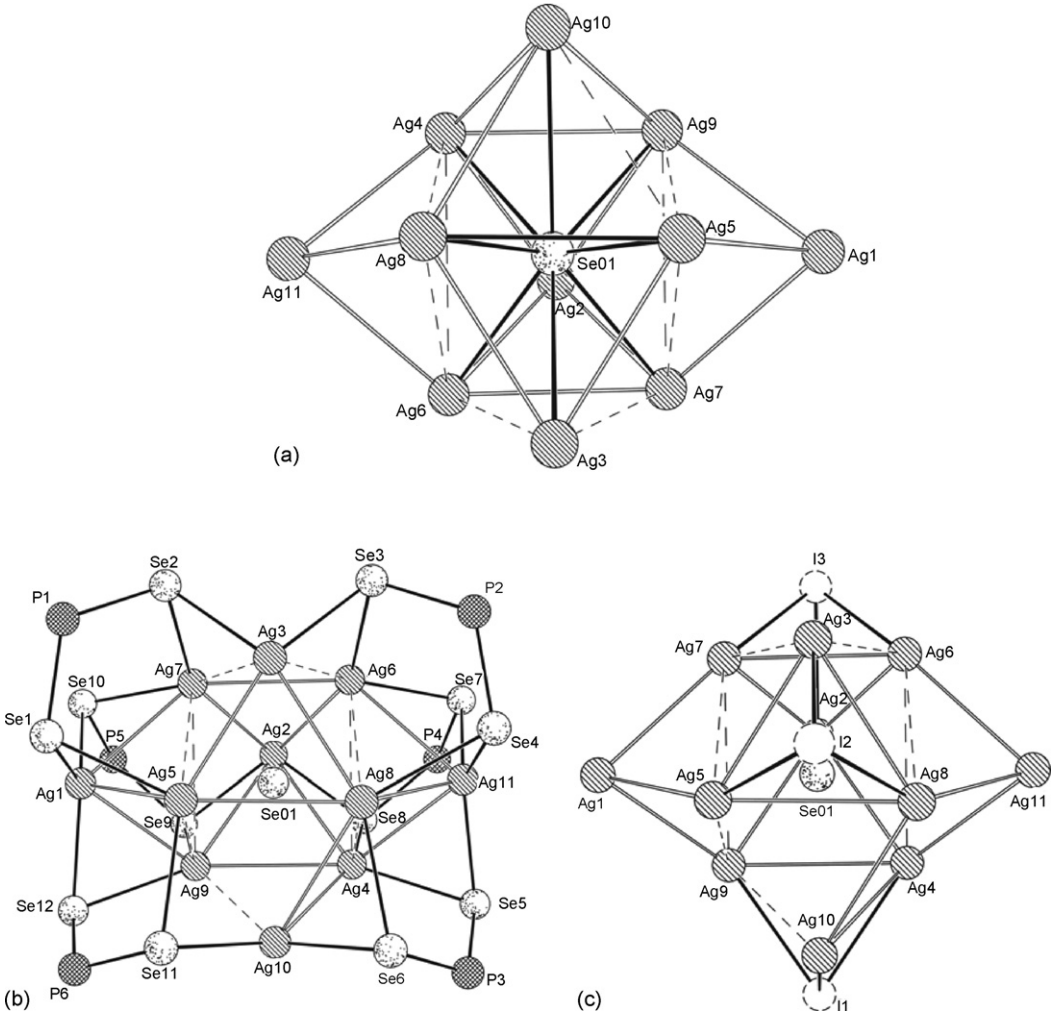

Fig. 14. (a) The $Ag_{11}Se$ core unit of cluster **30c**. (b) The $Ag_{11}Se$ core with the addition of six diisopropyl diselenophosphate ligands. The iso-propoxyl groups are omitted for clarity. (c) The drawing of $Ag_{11}Se$ core with the addition of three iodo ligands (adapted from Ref. [69]).

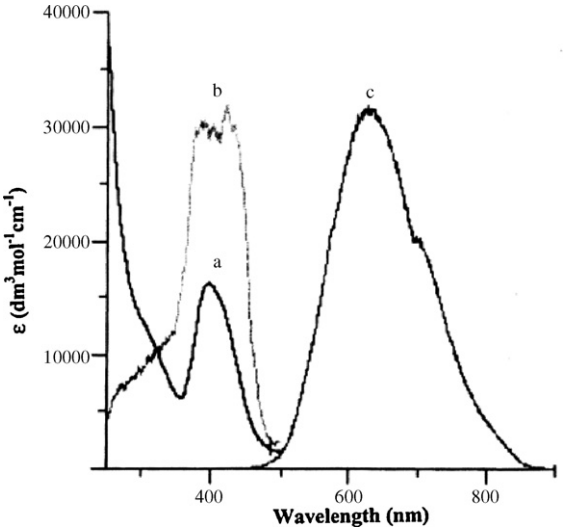

Fig. 15. (a) Electronic absorption spectrum, (b) excitation spectrum, and (c) emission spectrum of **30c** at 298 K (adapted from Ref. [69]).

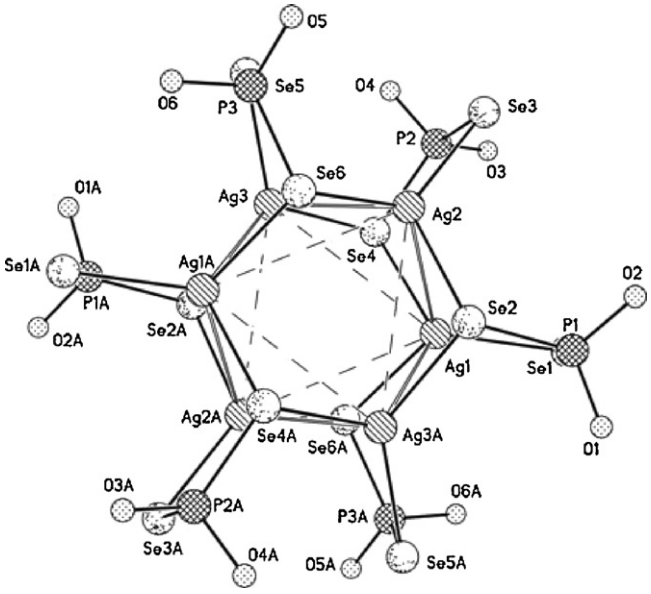

Fig. 16. Structure of $[Ag\{Se_2P(O^iPr)_2\}]_6$ **29c** with isopropyl groups omitted (adapted from Ref. [38]).

3.4.2.4. Selenide-centered undecanuclear clusters. Selenide-centered undecanuclear silver clusters $[Ag_{11}(\mu_9\text{-Se})(\mu_3\text{-I})_3\{Se_2P(OR)_2\}_6]$ (R = Et, *30a*, ^{i}Pr, **30c**, ^{2}Bu, **30d**) [69], capped by three iodo and six dsep ligands were successfully synthesized by using the method described in Eq. (11). They were fully characterized by NMR, FAB mass, UV–vis spectrometry, and two of them by X-ray diffraction. Eleven silver atoms adopt the geometry of 3,3,4,4,4-pentacapped trigonal prism with a central, nonacoordinated selenium atom in a tricapped trigonal prismatic geometry (Fig. 14a). The Ag–μ_9Se distances are in the range of 2.696–3.157 Å. There are six face-capped dsep ligands (Fig. 14b) along the three-fold axis, which goes through Ag1, Se(0 1), and Ag11 atoms, and three triply bridging, iodo ligands perpendicular to the C_3 (Fig. 14c). They are iso-structural with their copper counterparts except that several intermolecular Se···I interactions were identified. Interestingly, these clusters exhibit orange-red luminescence under UV-irradiation in both solid state and solution. The representative spectra of the isopropyl derivative which include absorption, excitation and emission at ambient temperature in solution are depicted in Fig. 15.

3.4.2.5. Hexanuclear cluster. Hexanuclear cluster $[Ag\{Se_2P(O^iPr)_2\}]_6$ **29c** along with Ag_{10} cluster 28c were formed as shown in Eq. (10) [38]. The single crystal X-ray study reveals that six Ag atoms of **29c** are located at the corners of a psuedohexagonal prism formed by alternating selenium atoms in two Ag_3Se_3 rings interconnected vertically by the P–Se groups of the dsep ligands (Fig. 16). The dsep ligands are organized in a paddle-wheel fashion about an Ag_6Se_6 psuedohexagonal prismatic core. The geometry of the Ag_6Se_{12} core revealed in **29c** with idealized D_{3d} symmetry, displays a distinct geometry compared to that of $[Ag_6\{Se_2P(O^iPr)_2\}_6]$, **25**, a S_6 point group symmetry found in part of the co-crystallization product as shown in Eq. (8). Cluster **29c** exhibits considerable Ag^I–Ag^I argentophilic interactions (3.047–3.152 Å).

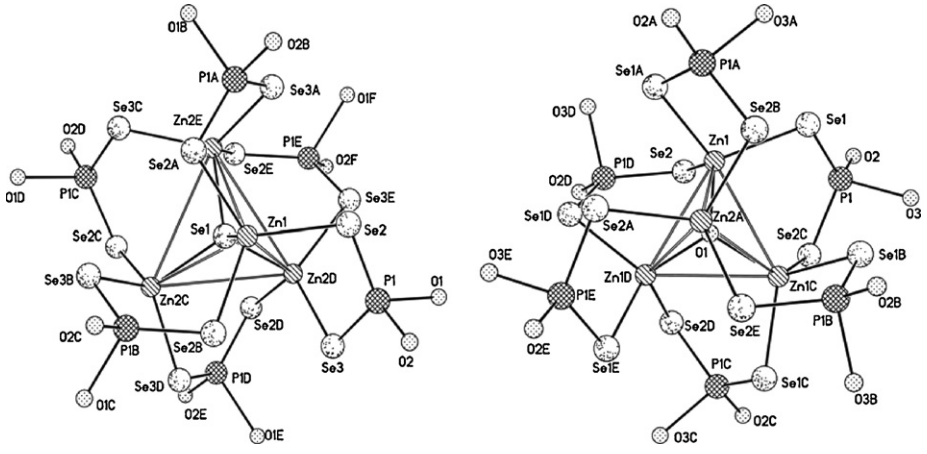

Fig. 17. Structures of $[Zn_4(\mu_4\text{-Se})\{Se_2P(O^nPr)_2\}_6]$ **31b** (left) and $[Zn_4(\mu_4\text{-O})\{Se_2P(OEt)_2\}_6]$ **32a** (right) with alkyl groups omitted for clarity (adapted from Refs. [71,72]).

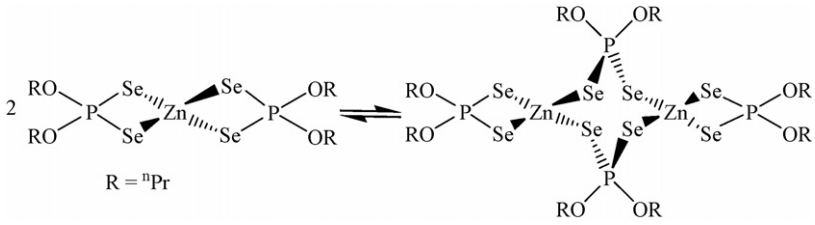

Scheme 1.

3.5. Group 12 elements (Zn, Cd, Hg)

Group 12 complexes which consist of dsep ligands and reported recently are depicted in Eqs. (12) and (13) [70–72]. Only a few preliminary reports about the formation of $Zn(Se_2PR_2)_2$ (R = Et, Ph, OEt), and $Cd(Se_2PR_2)_2$ (R = Ph, OEt) with no structural details appeared in the past [4,17,53]. Elements of this group prefer to form dimers, chalcogen-centered tetranuclear clusters, and polymers, a behavior different from that of group 11 metals, which formed clusters with higher nuclearity. The high prevalence of close metal–metal contacts in group 11 metals associated with their soft Lewis-acid behavior may be the main reasons for the apparent difference:

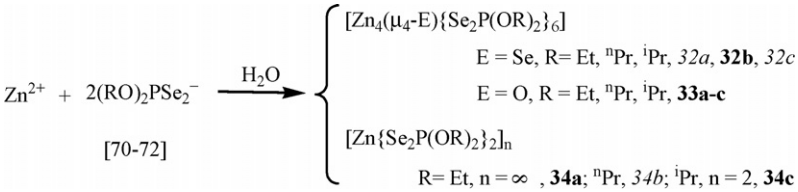

(12)

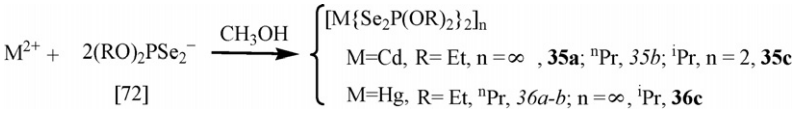

(13)

Zinc(II) has yielded two types of compounds: (i) Se-centered tetranuclear clusters, **31a–c**, and O-centered tetranuclear clusters, **32a–c** for R = Et, ^{n}Pr and ^{i}Pr, (ii) dinuclear or polymeric complexes, **33a–c**. Cadmium(II) and mercury(II) only formed either dimers or polymers (**34–35**) [70–72]. Se-centered tetranuclear zinc clusters are formed only when the reaction time is short usually within 5–10 min. The origin of oxygen atoms in clusters could be air or H_2O. Dimeric or polymeric compounds **33** were formed when the reaction time was longer than 2 h; there was no evidence for the formation of Se- or O-centered clusters in the case of Cd and Hg even though the reaction time was kept short. It is possible that Se-centered clusters of Cd and Hg are less stable. Thus their isolation becomes difficult.

Only one Se-centered tetranuclear zinc cluster could be structurally characterized (Fig. 17), though FAB-mass supported the formation of three such clusters for zinc. Zinc atoms in **31b** are located at the vertex of a regular tetrahedron with each edge bridged by a dsep ligand (mode **III**). Each zinc atom is tetragonally connected by three Se atoms from three dsep ligands and one central Se atom. VT NMR studies revealed that this cluster is partly decomposed to the monomer $[Zn\{Se_2P(O^nPr)_2\}_2]$, which showed exchange equilibrium with its dimer (Scheme 1). The ^{77}Se NMR at −80 °C showed the presence of the selenide-centered Zn_4 cluster along with bridging and chelating dsep ligands of the dimer because at this temperature the exchange stops and the monomer completely changes into the dimer.

Oxygen-centered clusters **32** are isostructural with selenium-centered clusters **31** [72]. Each zinc atom is coordinated by three selenium atoms from three bridging dsep ligands, and the fourth site is occupied by the central oxygen atom. The geometry around each Zn center is distorted tetrahedral. Similarly, the geometry at the central oxygen atom is slightly distorted from a perfect tetrahedral.

Compound $[Zn\{Se_2P(OEt)_2\}_2]_n$ **33a** is a one-dimensional helical chain polymer. One dsep ligand chelates to each zinc atom, and the second one bridges the two zinc atoms and this process continues to form a one-dimensional helical chain [70]. The geometry around each zinc center is distorted tetrahedral.

Dimeric compound $[Zn_2\{Se_2P(O^iPr)_2\}_4]$ **33c** has two dsep ligands bridging two zinc centers, and each zinc atom has one chelating dsep ligand (Fig. 18) [70]. VT NMR studies revealed that monomer and dimer of **33c** are in equilibrium in solution via the exchange of bridging and chelating ligands (similar to that shown in Scheme 1). At 40 °C, it exists essentially as monomer and at −90 °C it exists as a dimer.

The structure of dinuclear compound $Cd_2\{Se_2P(O^iPr)_2\}_4]$ **34c** is similar to that of zinc dimer **33c** (Fig. 19). The $Cd_2Se_4P_2$ eight-membered ring adopts a saddle-shape configuration and each cadmium atom is in a distorted tetrahedral geometry. Compound **34c** in CD_2Cl_2 showed monomer–dimer exchange equilibrium similar to that observed in $[Zn_2\{Se_2P(O^iPr)_2\}_4]$ **33c**.

In compound $[Cd\{Se_2P(OEt)_2\}_2]_\infty$ **34a**, two dsep ligands bridge two Cd atoms forming an eight-membered ring and it is a linear double-chain polymer. The eight-membered rings adopt criss-cross orientations (Fig. 20). On the other hand, in the zinc

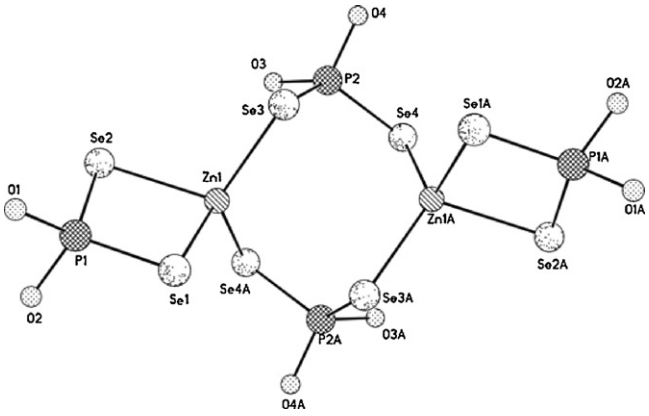

Fig. 18. Structure of $[Zn_2\{Se_2P(O^iPr)_2\}_4]$ **33c** (adapted from Ref. [70]).

polymer **33a**, one dsep bridges two zinc atoms and the other chelates a zinc atom, and in this way a helical chain was obtained. The geometry around Cd is distorted tetrahedral.

The bonding pattern in polymer $[Hg\{Se_2P(O^iPr)_2\}_2]_\infty$ **35c** (Fig. 21), is similar to that in zinc polymer **33a**, with the difference that the chelating dsep ligands are oriented on both sides of the helical chain vis-à-vis zinc polymer **33a**, in which all the chelating dsep ligands are oriented in one side. In both Hg polymer **35c**, and Zn polymer **33a**, the bridging and chelating dsep ligands co-exist unlike only bridging patterns observed in Cd polymer **34a**. The coordination geometry around Hg is distorted tetrahedral. Polymer **35c** undergoes depolymerization in $CDCl_3$ and exhibits monomer–dimer exchange equilibrium in the temperature range of 20 to −60 °C [72].

Reaction of cadmium(II) acetate with two moles of dsepo ligand, $Ph(RO)PSe_2^-$ yielded the complexes $[Cd_2\{Se_2P(OR)Ph\}_4]$ (R = Me, Et, ^{i}Pr, **36a**, *36b*, *36c*) [19]. The structure of **36a** shows that it exists as a dimer with two types of dsepo ligands, each bound to one Cd atom via both selenium atoms and the other acting as bridging ligands with their selenium atoms binding to two different Cd atoms to form an eight-membered ring similar to that of **34c**. The NMR studies suggest that equilibrium exists with rapid exchange between a monomeric and a dimeric species for complexes **36**.

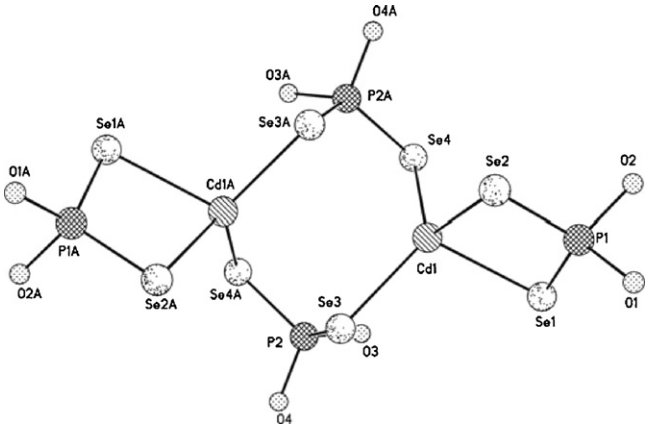

Fig. 19. Structure of $Cd_2\{Se_2P(O^iPr)_2\}_4]$ **34c** with isopropyl groups omitted (adapted from Ref. [72]).

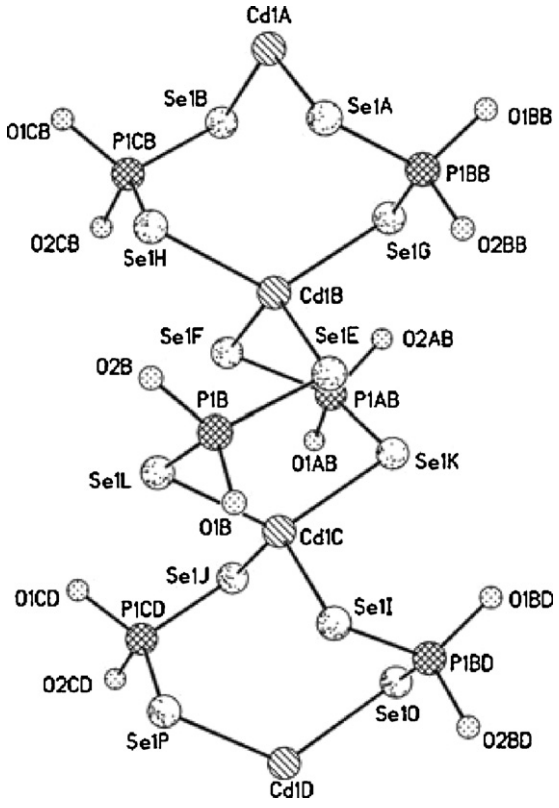

Fig. 20. Structure of $[Cd\{Se_2P(OEt)_2\}_2]_\infty$ **34a** (adapted from Ref. [72]).

3.6. Group 13–15 elements (In, Tl, Ge, Sn, Pb, As, Sb, Bi)

The complexes containing dsep ligand are depicted in Eqs. (14)–(16), and some of them are established by X-ray crystallography, and from allied ligands, only structures of $In(Se_2PPh_2)_3$ (**37**) [42] and $Tl(Se_2PEt_2)$ (**38**) [17,73], are known. Other compounds with no structure characterization are as follows: $M[Se_2P(OEt)_2]_2$ (M = Sn, Pb) [16], $Pb(Se_2PR_2)_2$ (R = Et [17], R = Ph [74]), $Tl[Se_2P(OEt)_2]$ [2], $In(Se_2PEt_2)_3$ [17], $Sb(Se_2PPh_2)_3$ [74], $Bi(Se_2PEt_2)_3$ [17], and $M[Se_2P(OEt)_2]_3$

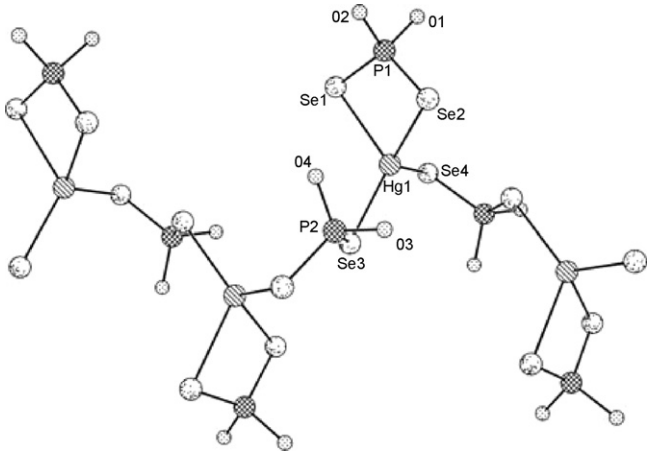

Fig. 21. Structure of $[Hg\{Se_2P(O^iPr)_2\}_2]_\infty$ **35c** with isopropyl groups omitted (adapted from Ref. [72]).

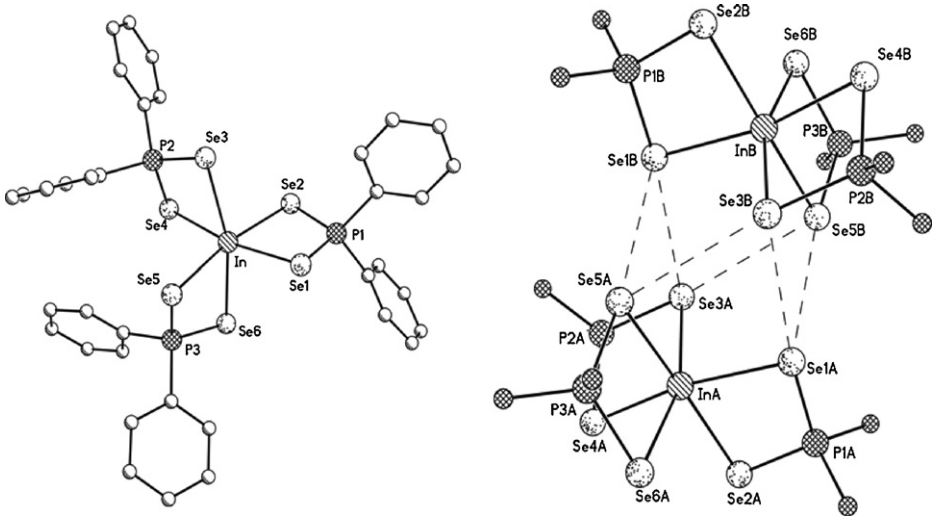

Fig. 22. Structure of $In(Se_2PPh_2)_3$ (**37**) (left), the Se···Se interactions in **37** (right) (adapted from Ref. [42]).

(M = As, Sb, and Bi) [2].

$$In^{3+} + 3[Se_2P(OR)_2]^- \xrightarrow[[75]]{CH_2Cl_2} In[Se_2P(OR)_2]_3,$$

R = Et, 40*a*; ^{i}Pr, **40c** (14)

$$Ph_3M^+ + [Se_2P(OR)_2]^- \xrightarrow{Et_2O} Ph_3M[Se(Se)P(OR)_2]$$

[76] R= Et, ^{n}Pr, ^{i}Pr, M = Ge, **41a**, *41b-c*; Sn, **42a-b**, *42c*; Pb, **43a,** *43b-c*

(15)

$$M^{3+} + 3[Se_2P(OR)_2]^- \xrightarrow{CH_2Cl_2} M[Se_2P(OR)_2]_3$$

[2] [49] R = Et, Pr, ^{i}Pr, M = Sb, *45a-b*, **45c**

R = Et, Pr, ^{i}Pr, M = Bi, *79d*, **46b** ,*46c*

(16)

Compound $In(Se_2PPh_2)_3$ (**37**) formed crystals in thf and toluene solvents. The geometry around indium center, which is chelated by three dsepi ligands, is distorted octahedral. The structure involves Se···Se interactions and forms a dimer (Fig. 22).

Compound $In[Se_2P(O^iPr)_2]_3$ **39c** is iso-structural with **37**. The indium atom surrounded by three dsep ligands is in distorted octahedral [75]. There also exist weak intermolecular interactions between Se atoms of the adjacent molecules. The Se···Se distances in **39c** are 3.533 Å, which is less than twice the sum of the van der Waals radius of Se atom, 4.0 Å. The VT ^{31}P NMR studies reveal that the In–Se bonds are labile in solution and undergo chelating-non-chelating ligand exchange.

There are several dsep derivatives of organogermanium(IV), tin(IV) and lead(IV); namely $[Ph_3M\{\eta^1\text{-}Se(Se)P(OR)_2\}]$ [R = Et, ^{n}Pr, ^{i}Pr, M = Ge, **40a**, 40*b–c*; Sn, **41a–b**, *41c*; Pb, **42a**, *42b–c*)] [76]. The crystal structures of **40a**, **41a**, **41b** and **42a**, showed that each metal is σ-bonded to three phenyl groups and one Se atom from the ligand. The dsep ligands are in monodentate coordination (η^1-Se) with one pendant Se atom (mode **I**). The geometry around metal center for each compound is distorted tetrahedral. A representative structure of **40a** is displayed in Fig. 23. The coordinated P–Se bond is longer as expected, than the pendant P–Se bond (cf. P–Se, single bond, 2.32 Å). The solution state (^{31}P and ^{77}Se NMR) studies have revealed that while germanium compounds do not show lability of Ge–Se bonds, the Sn and Pb compounds do exhibit lability of Sn–Se and Pb–Se bonds, which involve exchange of the coordinated and pendant Se atoms at room temperature (Scheme 2). This exchange process is slowed down at low temperature and stopped at around 210 K. Positive FAB-mass spectra and density functional theory

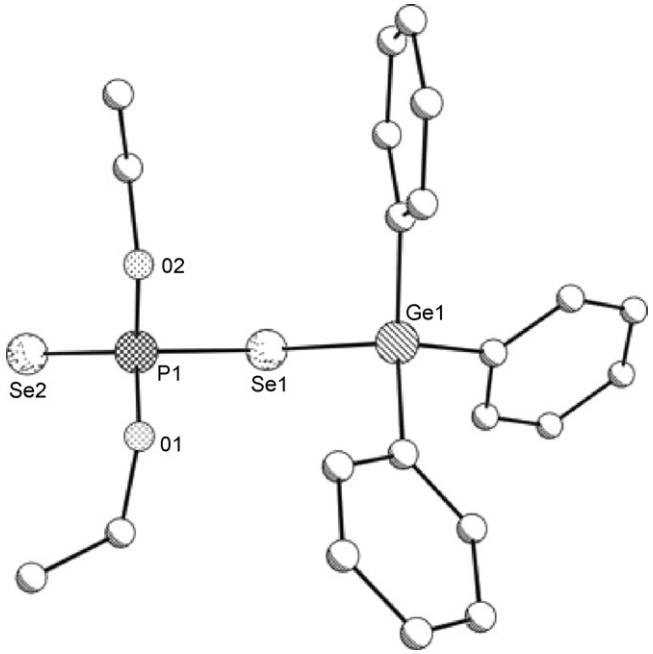

Fig. 23. Molecular structure of $[(C_6H_5)_3Ge\{\eta^1\text{-}Se(Se)P(OEt)_2\}]$, **40a** (adapted from Ref. [76]).

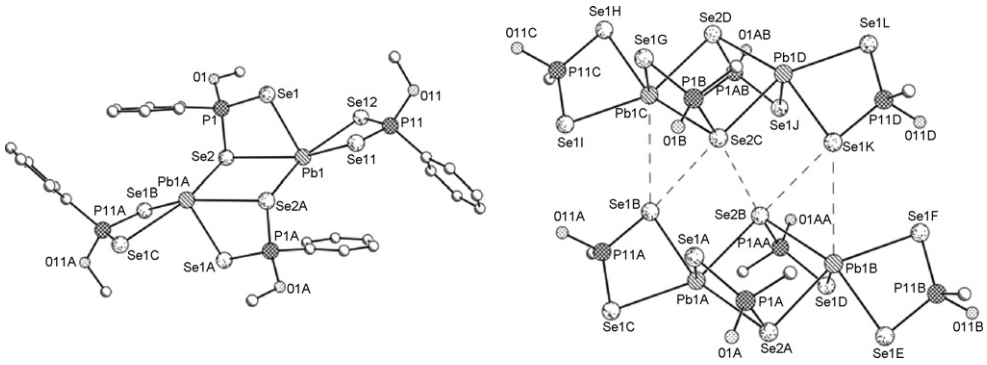

Fig. 24. Structure of $[Pb_2\{Se_2P(OMe)Ph\}_4]$ **44a** (left), crystal packing depicting Se···Se and Pb···Se interactions (right) (adapted from Ref. [19]).

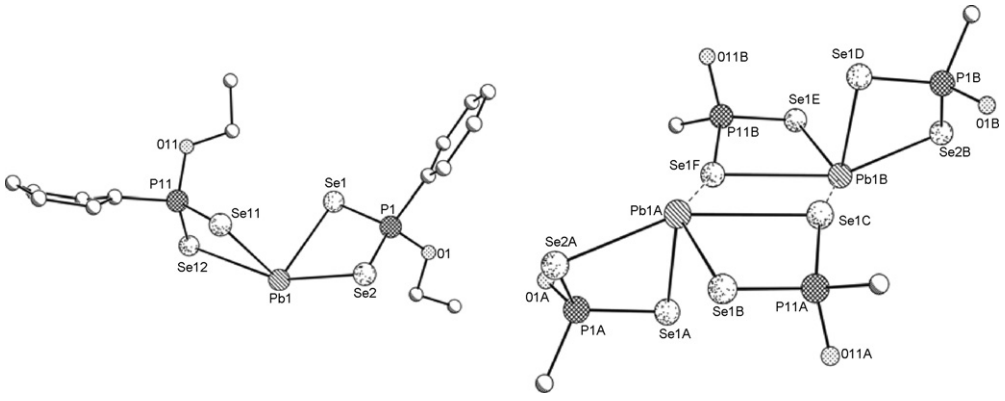

Fig. 25. Structure of $[Pb\{Se_2P(OEt)Ph\}_2]$ **44b** (left), pair of units forming a dimeric structure (right) (adapted from Ref. [19]).

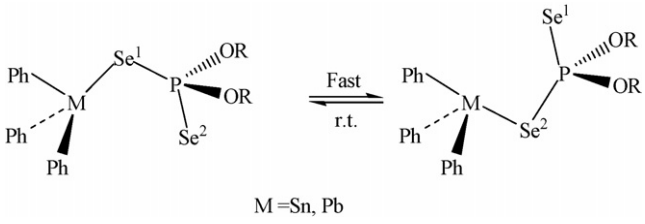

Scheme 2.

support the formation of monomers as well as unusual dinuclear cations $[(Ph_3M)_2\{\mu\text{-Se, Se-P(OR)}_2\}]^+$ [76].

Reactions of tin(II) dichloride and lead(II) acetate with two moles of dsepo ligand, $Ph(RO)PSe_2^-$ yielded the complexes $[M\{Se_2P(OR)Ph\}_2]$ (M, R: Sn, Me, *43*; Pb, Me, Et, ^{i}Pr, **44a–b**, *44c*) [19]. Compound **44a** exists as a dimer, and its structure is shown in Fig. 24. It has a central Pb_2Se_2 ring and each Pb has a distorted trigonal bipyramid geometry formed by chelating and bridging dsepo ligands. Each Pb atom is chelated by two dsepo ligands to presumably form a monomeric unit $[Pb\{Se_2P(OMe)Ph\}_2]$, and two units of this monomer dimerize

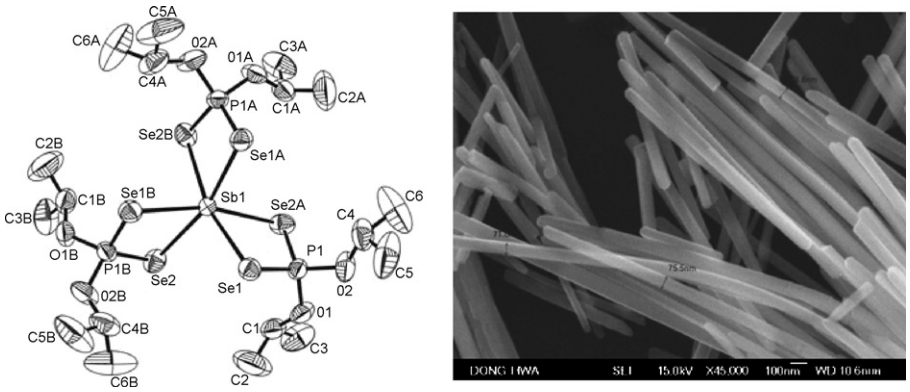

Fig. 26. Structure of **45c** (left), SEM image of Sb_2Se_3 nanorods (right) (adapted from Ref. [49]).

via two Pb–Se bonds. The ligands adopt the terminal, bidentate chelating (mode **II**) as well as chelating, bridging coordination mode (mode **VIII**). The dimeric units of **44a** are weakly held together in a network of Pb···Se and Se···Se interactions in the solid state. The structure of **44b** (Fig. 25) shows that Pb has a distorted trigonal bipyramid geometry with a vacant site which provides for weak Pb···Se interactions (3.39 Å), leading to the formation of an eight-membered quasi-cyclic species. The NMR (^{31}P) spectra of both show a singlet with a pair of satellites and likewise in ^{77}Se, they show a doublet in each case.

Tris-chelated, dsep complexes of antimony and bismuth were synthesized from $Sb(CH_3COO)_3$ and $Bi(NO_3)_3$ with three equiv. of $NH_4Se_2P(OR)_2$ in CH_2Cl_2, respectively (Eq. (16)). Structures of **45c** and **46b** are known [49]. A typical distorted, octahedral metal center surrounded by six selenium atoms from three dsep ligands is revealed (Fig. 26). The secondary Se···Se interactions also exist to form a dimer in the solid state. By taking advantage of the ease P–Se bond cleavage of the dsep ligand, these compounds are excellent single source precursors for the fabrication of both antimony selenide and bismuth selenide nanomaterials by utilizing solvothermal method. One of the SEM images of Sb_2Se_3 nanorods is displayed in Fig. 26.

4. Conclusions and future outlook

From the survey and analysis of the research work described in this review, it may be appropriate to suggest some future guidelines for carrying out research activity. As regards dsep ligands, it appears appropriately to systematically investigate: (i) the role of a solvent on reaction course by using a series of solvents keeping molar ratio constant, (ii) the role of molar ratio on nature of product by keeping solvent constant, (iii) effect of temperature on the course of a reaction with a given solvent, (iv) effect of counter anion of the metal ion on the nature of product. These four operations will help standardize the resulting products and can be useful in preferential preparation a desired compound. These experiments can be extended to other types of ligand as well. This will develop a background for crystal engineering. Apart from the above-mentioned experiments, metal complexes of dsep and allied ligands can be exploited for the fabrication of semiconductors based on metal selenides in the form of nanostructures. This would lead to investigate the thermal behavior of compounds using TGA, DTA, DSC, and in suitable cases using CVD or simple solvothermal method for nanomaterials. The photophysical behavior of compounds can be another interesting area. The use of linkers such as 4,4′-bipyridine can be useful in making conducting polymers. Supramolecular chemistry based on Se···Se interactions provides another interesting area of research useful for semiconducting materials.

The coordination of chemistry of ligands with PSe_2 and PSe_3 functional groups investigated so far is limited as compared to their sulfur analogs and in view of available synthetic methods for the preparation of ligands, it is believed that future investigations will focus on these selenium-based ligands. It becomes all the more tempting to pursue research in this area when ligands such as dsep have yielded clusters and polymers, some of which have no parallel, to show lability of P–Se and M–Se bonds, depolymerization, monomer-dimer exchange equilibrium, variable bonding modes, etc. It is believed that this review article describing the coordination chemistry of dsep and allied ligands will become a platform for future investigations to the development of chalcophosphate metal complexes with potential applications.

Acknowledgements

I would like to thank my co-workers especially for Mr. Ben-Jie Liaw who provides most of the figure drawings. Our research was supported by The National Science Council of Taiwan (NSC 94-2113-M-259-010).

References

[1] M.V. Kudchadker, R.A. Zingaro, K.J. Irgolic, Can. J. Chem. 46 (1968) 1415.
[2] V. Krishnan, R.A. Zingaro, Inorg. Chem. 8 (1969) 2337.
[3] A.A.G. Tomlinson, J. Chem. Soc. A (1971) 1409.
[4] V. Krishnan, R.A. Zingaro, J. Coord. Chem. 1 (1971) 1.
[5] G.M. Larin, E. Dyatkina, Izv. Akad. Nauk. SSR Ser. Khim. 6 (1972) 1413.
[6] I. Haiduc, D.B. Sowerby, S.-F. Lu, Polyhedron 14 (1995) 3389.
[7] C.W. Liu, J.T. Pitts, J.P. Fackler Jr., Polyhedron 16 (1997) 3899.
[8] J.P. Fackler Jr., R.J. Staples, C.W. Liu, R.T. Stubs, C. Lopez, J.T. Pitts, Pure Appl. Chem. 70 (1998) 839.
[9] J.P. Fackler Jr., Inorg. Chem. 41 (2002) 6959.
[10] D. Wu, J.-Q. Huang, Y. Lin, J.-L. Haung, Sci. Sin. Ser. B (Engl. ed.) 31 (1988) 800.
[11] R. Wasson, G.M. Woltermann, H.J. Stoklosa, Fortschr. Chem. Forsch. (Top. Curr. Chem.) 35 (1973) 65.
[12] R.C. Mehrotra, G. Srivastava, B.P.S. Chauhan, Coord. Chem. Rev. 55 (1984) 207.
[13] K.C. Molloy, J.J. Zuckerman, Acc. Chem. Res. 16 (1983) 386.
[14] E.R.T. Tiekink, Main Group Met. Chem. 15 (1992) 161.
[15] B.-J. Liaw, T.S. Lobana, Y.-W. Lin, J.-C. Wang, C.W. Liu, Inorg. Chem. 44 (2005) 9921.
[16] C.W. Liu, H.-C. Chen, J.-C. Wang, T.-C. Keng, Chem. Comm. (1998) 1831.
[17] W. Kuchen, B. Knop, Angew. Chem. Int. Ed. Engl. 4 (1965) 244.
[18] I.P. Parkin, M.J. Pilkington, A.M.Z. Slawin, D.J. Williams, J.D. Woollins, Polyhedron 9 (1990) 987.
[19] I.P. Gray, A.M.Z. Slawin, J.D. Woollins, Dalton Trans. (2005) 2188.
[20] D. Fenske, in: G. Schmid (Ed.), Clusters and Colloids—From Theory to Applications, D. VCH, Weinheim, Germany, 1994.
[21] C.W. Liu, R.T. Stubs, R.J. Staples, J.P. Fackler Jr., J. Am. Chem. Soc. 117 (1995) 9778.
[22] Z.X. Huang, S.F. Lu, J.Q. Huang, D.M. Wu, J.L. Huang, J. Struct. Chem. 10 (1991) 213.
[23] I.G. Dance, R. Garbutt, D. Craig, Inorg. Chem. 26 (1987) 3732.
[24] H.B. Burgi, H. Gehrer, P. Strickler, F.K. Winkler, Helv. Chim. Acta 59 (1976) 2558.
[25] (a) C.W. Liu, M.D. Irwin, A.A. Mohamed, J.P. Fackler Jr., Inorg. Chim. Acta 357 (2004) 3950;
(b) K. Matsumoto, R. Tanaka, R. Shimomura, Y. Nakao, Inorg. Chim. Acta 304 (2000) 293.
[26] R.A. Wheeler, J. Am. Chem. Soc. 112 (1990) 8737.
[27] E. Furet, A. Le Beuze, J.-F. Halet, J.-Y. Saillard, J. Am. Chem. Soc. 117 (1995) 4936.
[28] M.T. Garland, J.-F. Halet, J.-Y. Saillard, Inorg. Chem. 40 (2001) 3342.
[29] R. Gautier, F. Ogliaro, J.-F. Halet, J.-Y. Saillard, E. Baerends, Eur. J. Inorg. Chem. (1999) 1161.
[30] R. Gautier, J.-F. Halet, J.-Y. Saillard, Eur. J. Inorg. Chem. (1999) 673.
[31] B. Zouchoune, F. Ogliaro, J.-F. Halet, J.-Y. Saillard, J.R. Eveland, K.H. Whitmire, Inorg. Chem. 37 (1998) 865.

[32] E. Furet, A. Le Beuze, J.-F. Halet, J.-Y. Saillard, J. Am. Chem. Soc. 116 (1994) 274.
[33] B. Sarkar (Ed.), Genetic Response to Metals, Dekker, New York, 1995.
[34] M.C. Linder, C.A. Goode (Eds.), Biochemistry of Copper, Plenum Press, New York, 1991.
[35] C.W. Liu, I.-J. Shang, J.-C. Wang, T.-C. Keng, Chem. Comm. (1999) 995.
[36] C.W. Liu, C.-M. Hung, H.-C. Chen, J.-C. Wang, T.-C. Keng, K. Guo, Chem. Comm. (2000) 1897.
[37] C.W. Liu, H.-C. Chen, J.-C. Wang, T.-C. Keng, Angew. Chem. Int. Ed. 40 (2001) 2342.
[38] C.W. Liu, I.-J. Shang, C.-M. Hung, J.-C. Wang, T.-C. Keng, J. Chem. Soc. Dalton Trans. (2002) 1974.
[39] W. Kuchen, H. Hertel, Angew. Chem, Int. Ed. Engl. 8 (1969) 89.
[40] R.P. Davis, M.G. Martinelli, Inorg. Chem. 41 (2002) 348.
[41] K. Karaghiosoff, K. Eckstein, Phosphorus Sulfur Silicon Relat. Elem. 75 (1993) 257.
[42] R.P. Davis, C.V. Francis, A.P.S. Jurd, M.G. Martinelli, A.J.P. White, D.J. Williams, Inorg. Chem. 43 (2004) 4802.
[43] M.J. Pilkington, A.M.Z. Slawin, D.J. Williams, J.D. Woollins, Polyhedron 10 (1991) 2641.
[44] L. Gelmini, D.W. Stephan, Organometallics 6 (1987) 1515.
[45] W. Kuchen, B. Knop, Chem. Ber. 99 (1966) 1663.
[46] H. Hertel, W. Kuchen, Chem. Ber. 104 (1971) 1740.
[47] H. Hertel, W. Kuchen, Chem. Ber. 104 (1971) 1735.
[48] Z.R. Baratova, P.M. Solozhenkin, E.V. Semenov, Ya.I. Mel'nik, O.N. Grishina, Dok. Akad. Nauk. Tadz. SSR 22 (1979) 478.
[49] C.W. Liu, Unpublished results.
[50] V. Bereau, J.A. Ibers, C.R. Acad. Sci. Ser. IIC Chim. 3 (2000) 123.
[51] R.D. Shannon, Acta Crystallogr. A32 (1976) 751.
[52] Q.-F. Zhang, F.K.M. Cheung, W.-Y. Wong, I.D. Williams, W.-H. Leung, Organometallics 20 (2001) 3777.
[53] A. Muller, P. Christophliemk, V.V. Krishna Rao, Chem. Ber. 104 (1971) 1905.
[54] L. Gastaldi, P. Porta, Cryst. Struct. Comm. 6 (1977) 175.
[55] T.A. Annan, R. Kumar, D.G. Tuck, J. Chem. Soc. Dalton Trans. (1991) 11.
[56] P.J.H.A.M. Leemput, T.W. Hummelink, J.H. Noordik, P.J. Beurskens, Crystal Struct. Comm. 4 (1975) 167.
[57] R. Das, B.S. Prabhananda, J. Magn. Reson. 54 (1983) 89.
[58] Y.-J. Hsu, C.-M. Hung, Y.-F. Lin, B.-J. Liaw, T.S. Lobana, S.-Y. Lu, C.W. Liu, Chem. Mater. 18 (2006) doi:10.1021/cm060478n, in press.
[59] C.W. Liu, C.-M. Hung, J.-C. Wang, T.-C. Keng, J. Chem. Soc. Dalton Trans. (2002) 3482.
[60] C.W. Liu, C.-M. Hung, B.K. Santra, Y.-H. Chu, Z. Lin, Inorg. Chem. 43 (2004) 4306.
[61] D. Fenske, H. Krautscheid, Angew. Chem. Int. Ed. Engl. 29 (1990) 1452.
[62] A. Deveson, S. Dehnen, D. Fenske, J. Chem. Soc. Dalton Trans. (1997) 4491.
[63] C.W. Liu, C.-M. Hung, B.K. Santra, H.-C. Chen, H.-H. Hsueh, Inorg. Chem. 742 (2003) 3216.
[64] A. Bondi, J. Phys. Chem. 68 (1964) 441.
[65] J.E. Huheey, E.A. Keiter, R.L. Keiter, Inorganic Chemistry: Principals of Structure and Reactivity, fourth ed., Harper Collins College, Publishers, New York, 1993.
[66] C.W. Liu, C.-M. Hung, B.K. Santra, J.-C. Wang, H.-M. Kao, Z. Lin, Inorg. Chem. 42 (2003) 8551.
[67] C.W. Liu, C.-M. Hung, H.-C. Haia, B.-J. Liaw, L.-S. Liou, Y.-F. Tsai, J.-C. Wang, Chem. Comm. (2003) 976.
[68] C.W. Liu, H.-C. Haia, C.-M. Hung, B.K. Santra, B.-J. Liaw, Z. Lin, J.-C. Wang, Inorg. Chem. 43 (2004) 4464.
[69] C.W. Liu, I.-J. Shang, R.-J. Fu, B.-J. Liaw, J.-C. Wang, I.-J. Chang, Inorg. Chem. 45 (2006) 2335.
[70] B.K. Santra, B.-J. Liaw, C.-M. Hung, C.W. Liu, Inorg. Chem. 42 (2003) 8866.
[71] B.K. Santra, C.-M. Hung, B.-J. Liaw, J.-C. Wang, C.W. Liu, Inorg. Chem. 43 (2004) 7570.
[72] C.W. Liu, T.S. Lobana, B.K. Santra, C.-M. Hung, H.-Y. Liu, B.-J. Liaw, J.-C. Wang, Dalton Trans. (2006) 560.
[73] A. Muller, V.V.K. Rao, P. Christophliemk, J. Inorg. Nucl. Chem. 36 (1974) 472.
[74] S. Esperas, S. Husebye, Acta Chem. Scand. 27 (1973) 1827.
[75] J.-M. Chen, B.K. Santra, C.W. Liu, Inorg. Chem. Comm. 7 (2004) 1103.
[76] C.W. Liu, T.S. Lobana, J.-L. Xiao, H.-Y. Liu, B.-J. Liaw, C.-M. Hung, Z. Lin, Organometallics 24 (2005) 4072.